Available online at www.sciencedirect.com
ScienceDirect
Journal of Sound and Vibration 313 (2008) 696–722
JOURNAL OF SOUND AND VIBRATION
www.elsevier.com/locate/jsvi

Absolute and relative path measures in a discrete system by using two analytical methods

A. Inoue, R. Singh*, G.A. Fernandes

Acoustics and Dynamics Laboratory, Department of Mechanical Engineering, and Center for Automotive Research, The Ohio State University, Columbus, OH 43210, USA

Received 16 April 2006; received in revised form 4 September 2007; accepted 18 September 2007
Handling Editor: C. Morfey
Available online 31 January 2008

Abstract

This paper analytically examines two vibration paths rank ordering methods and critically investigates several path identification issues. One method is the indirect interfacial path force estimation procedure that is employed in the well known experimental transfer path analysis. The other method is path disconnect scheme that has been historically utilized in industry to empirically find a dominant or defective path. In this article we utilize simplified, but pedagogical, discrete vibratory systems to clarify the underlying principles of both methods and to assess the path rank orders. Our analysis is limited to a linear time-invariant system (with only translating motions) under harmonic excitation and three distinct parallel paths (with or without masses) are considered. Alternate formulations of the interfacial path forces, based on direct and indirect methods, are derived. The indirect, yet exact, interfacial (path) force expressions could be used to estimate time-averaged dissipated power and Lagrangian energy spectra in various sub-systems. Estimations using only the driving point frequency response functions are emphasized, since they would ease the experimental burden. Next, the path disconnect method is analytically formulated and related to the path connect scheme (assuming one path at a time). This analysis reveals some useful relations among the path measures and the way a particular path could be connected or disconnected. A laboratory experiment validates the simplified massless path model, which yields asymptotic trends. Finally, all of the path rank orders are quantified and compared using many absolute and relative measures (based on interfacial force, receiver motion and sub-system energy relationships). Direction for future work is briefly discussed.

1. Introduction

Lately there has been considerable interest in the vibration transfer path analysis (TPA) [1–6], especially the identification of structure-borne noise paths [7–11], since the industrial design practice demands an unambiguous answer to the perennial question: Which paths are the most dominant? Traditionally, practitioners have attempted to determine the relative contribution of parallel paths by disconnect one path at a time and then measuring the resulting structural motions or sound pressures spectra, say at the receiver, in the practical system under realistic loads. In such empirical investigations, boundary and interfacial conditions

*Corresponding author. Tel.: +1 614 292 9044; fax: +1 614 292 3163.
E-mail address: singh.3@osu.edu (R. Singh).

0022-460X/$ - see front matter © 2007 Elsevier Ltd. All rights reserved.
doi:10.1016/j.jsv.2007.09.058

may vary from one to another experiment and consequently, path disconnect type experiments often do not seem to yield meaningful conclusions and in some cases the results may even frustrate the investigators. In our literature search, we could not find any scientific article that specifically discuss the path disconnect issues though that particular scheme (or its variation) has been employed in many industries on a regular basis for decades. To fill this void, we will examine the underlying concepts and intricacies associated with the path disconnect scheme in this paper by developing a simplified five degrees-of-freedom (dof) linear vibratory system model, as shown in Fig. 1. We will restrict our analysis to only three or two parallel structure-borne paths (P) between a single source (S) and a single receiver (R) though many interesting combinations exist in real life [4,6].

Alternately, we could employ the transfer path analysis, which is a relatively new approach to the path identification or rank-ordering problem [8–13]. It should be noted that the transfer path analysis is primarily an experimental method [14–17], though it could require considerable measurement effort. In particular, we recently conducted a comparative path rank ordering study by using a laboratory source–path–receiver (S–P–R) system based on the transfer path analysis concept [12]. In our experiment the vibration from the source chamber was transmitted to receiver location through three mounts that acted as parallel paths. The interfacial path forces and sound pressure were indirectly estimated by several methods, which were then compared with direct measurements. Nevertheless, our experimental study did not yield consistent rank orders of three structural paths. This has suggested that we must analytically examine the transfer path analysis procedure and thereby determine the plausible sources of error that may occur in a purely experimental study. Accordingly we will employ the key five degrees-of-freedom system example of Fig. 1 to critically assess the path identification issues and to compare the rank orders that could be obtained by using two analytical methods (namely the transfer path analysis and path disconnect scheme). Both absolute and relative path measures, such as the interfacial forces [18–21], power flow [22–25], and the insertion losses, would be utilized to quantity the parallel paths.

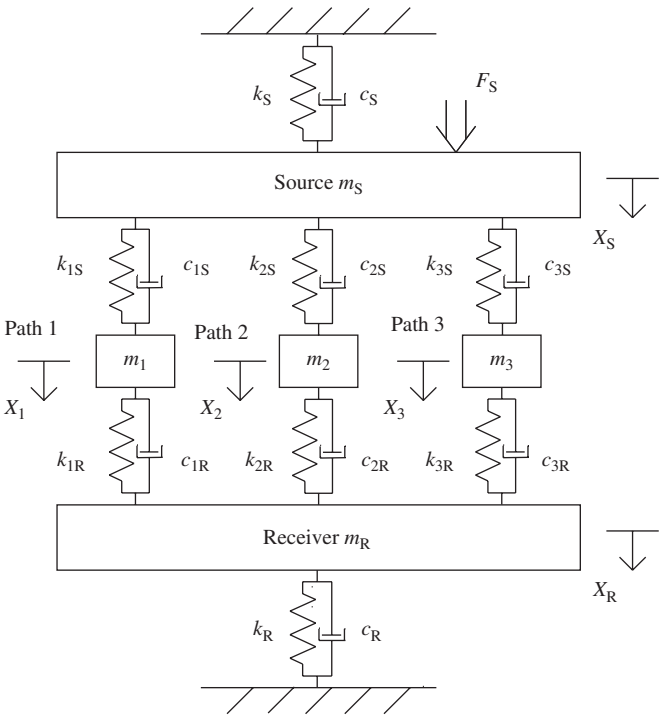

Fig. 1. Key example: five degrees-of-freedom mechanical system depicting three parallel paths (P), single source (S) and single receiver (R). Each path is assumed to possess mass as shown. Viscous damping element is associated with each spring.

2. Problem formulation

Only translational motions (in the vertical direction) are considered for a linear time-invariant five degrees-of-freedom system as shown in Fig. 1. Our analysis is restricted to the frequency domain as an external harmonic force $F_S e^{i\omega t}$ (frequency ω in rad/s) is applied to the source mass m_S. Forces are then transmitted into the receiver mass m_R through three (or two in some cases) parallel paths (with or without masses) as described below. The source and receiver masses are connected by Voight type visco-elastic paths. Thus, the complex stiffness concept at ω is used: $\tilde{k} = k + j\omega c$, where k is the storage stiffness and c is the related viscous damping coefficient. Since the chief objective of this paper is to provide a theoretical foundation of the multiple vibration transmission path analysis, we employ the two representative examples of Figs. 1 and 2, though

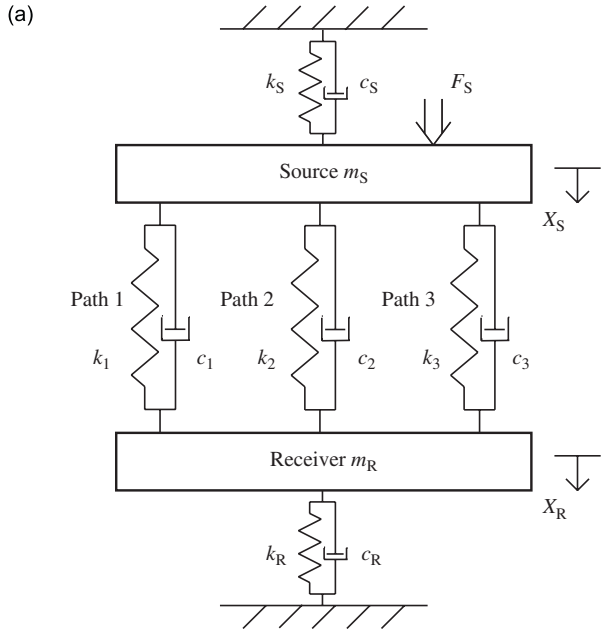

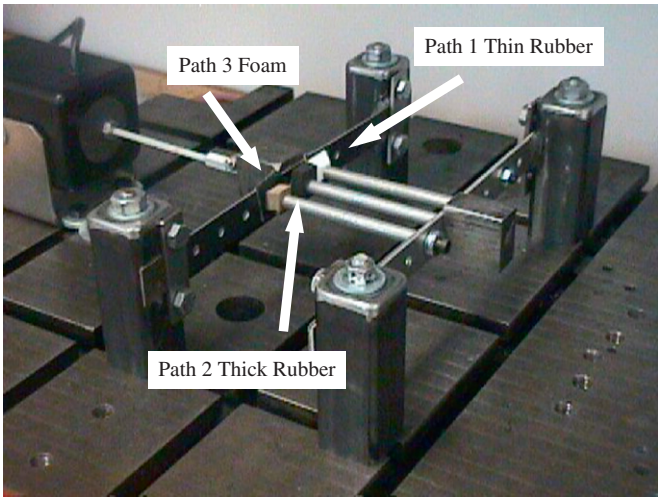

Fig. 2. Discrete mechanical system with three parallel massless paths. (a) two degrees-of-freedom analytical system; (b) analogous experiment. Three different isolators are inserted on the source side of each path in (b): 7 mm rubber in Path 1 (right), 10 mm rubber in Path 2 (center) and 8 mm foam in Path 3 (left).

many real-life systems would require more detailed discretized models. The five degrees-of-freedom system (with three path masses) is first studied computationally. Then analytical solutions are obtained for a four degrees-of-freedom system (with two parallel paths with masses); Path 3 in Fig. 1 is completely removed. Further, Fig. 2(a) shows a special case of a two degrees-of-freedom system (with three massless paths) since some practical path systems, including the engine mounts [3,25], have been described without any mass elements. Fig. 2(b) shows an analogous experiment that is used to simulate the two degrees-of-freedom system of Fig. 2(a). Unless otherwise specified, the five degrees-of-freedom system of Fig. 1 is considered in our analysis.

In order to correctly estimate the interfacial path forces in the transfer path analysis [8], the source structure has to be completely removed from the system in order to obtain the frequency response functions of the downstream sub-system. On the other hand, a traditional method of path rank ordering would connect only one path at a time, and compare the resulting response with that of the system with all paths; this is designated as the α scheme in our work, as depicted in Fig. 3(a). Alternatively we could sequentially remove or disconnect only one path at a time and then observe changes in the receiver responses; we call this method as the β scheme as shown in Fig. 3(b). It is interesting to note that when the ith path is disconnected, several boundary conditions corresponding to that path are possible.

For the sake of illustration, we will investigate the following five path disconnect methods as shown in Fig. 3(c). There are: remove the path completely (CM); disconnect on the source side and ground the end (SG); disconnect on the receiver side and ground the end (RG); disconnect on the source side and leave it free (SF); and disconnect on the receiver side and leave it free (RF). Consequently, in our nomenclature "α Path 1 with SG" (given by the subscripts α1: SG) means that only Path 1 is connected and all other paths are disconnected on the source side and then grounded. Further, the subscript "All" indicates the all paths are still connected.

An analysis of the different disconnect methods is needed because they could sometimes lead to erroneous results. For instance, a path disconnect scheme could significantly change the eigensolutions of the system. Therefore, we illustrate the above-mentioned concepts using the examples of Figs. 1–3 and provide an analytical foundation for evaluating the competing path rank ordering methods.

Specific objectives of this paper are as follows. First, to establish indirect (yet exact) interfacial (path) force estimation methods (used in transfer path analysis) with free or blocked boundary type frequency response functions of the sub-system. Estimations which require only the driving point frequency response functions are

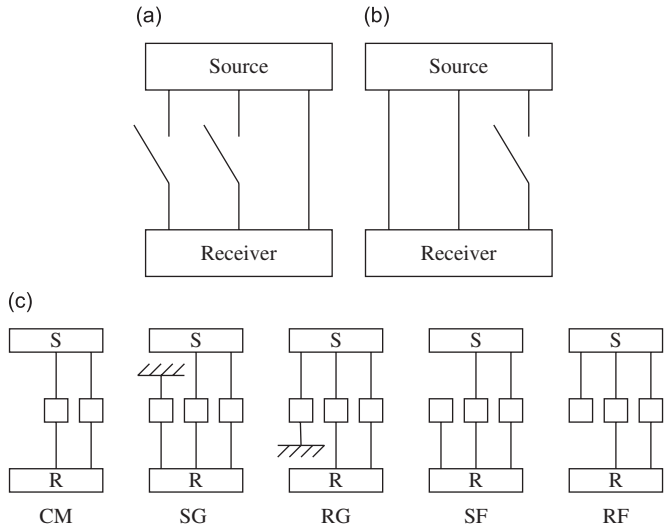

Fig. 3. Path connect and disconnect methods used to rank order paths. (a) α scheme-only the ith path is connected, but other paths are disconnected; (b) β scheme-only the ith path is disconnected, but other paths are still connected; (c) five ways of disconnecting the ith path: remove the path completely (CM); disconnect on the source side and ground the end (SG); disconnect on the receiver side and ground the end (RG); disconnect on the source side and leave it free (SF); disconnect on the receiver side and leave it free (RF).

emphasized. We will analytically and computationally compare indirect and direct force estimation methods. Second, to examine the path disconnect (β) and connect (α) methods analytically and find interrelationships between the two schemes and some path measures based on the simplified system models. Finally, to quantify and rank order the paths based on absolute and relative measures including energy-based calculations. In particular, we will compare path rank orders by the interfacial forces (which are required in transfer path analysis) and the path disconnect schemes (with basic system responses).

We begin the analytical treatment by recognizing that the parallel paths control the frequency response functions and eigensolutions. Since paths themselves are considerably and non-proportionally damped, one must use complex eigensolutions and/or the indirect matrix inversion methods to predict the frequency response of the system. The governing equations of motion (in frequency domain) are given in matrix form as

$$[\tilde{\mathbf{K}} - \omega^2\mathbf{M}]\mathbf{X} = \mathbf{F}, \tag{1}$$

where $\mathbf{M}$, $\tilde{\mathbf{K}} = \mathbf{K} + \mathrm{j}\omega\mathbf{C}$ and $\mathbf{C}$ are, respectively, the mass, complex stiffness and viscous damping matrices of the discrete system of dimension (or degrees-of-freedom) N. The ubiquitous $\mathrm{e}^{\mathrm{j}\omega t}$ terms are omitted in this paper for the sake of brevity. Bold symbols indicate matrix or vector. Hysteretic (structural) damping could replace the viscous damping by using: $\tilde{\mathbf{K}}' = \mathbf{K} + \mathrm{j}\mathbf{C}_{\mathrm{hysteretic}}$ instead. For the five degrees-of-freedom system (Fig. 1), the displacement amplitude vector is $\mathbf{X} = (X_S, X_1, X_2, X_3, X_R)^{\mathrm{T}}$, and the external harmonic force amplitude vector is $\mathbf{F} = (F_S, 0, 0, 0, 0)^{\mathrm{T}}$. Define the response in frequency domain as

$$\mathbf{X} = \mathbf{Z}^{-1}\mathbf{F} = \mathbf{H}\mathbf{F}, \tag{2}$$

where $\mathbf{H}$ and $\mathbf{Z}$ ($= \tilde{\mathbf{K}} - \omega^2\mathbf{M}$) are the dynamic compliance and dynamic stiffness matrices respectively. Eq. (2) is used for analytical calculations in later sections. Further, we employ the generalized (complex) modal expansion for the sake of computational efficiency [26].

$$\mathbf{X} = \sum_{r=1}^{2N} \frac{\mathbf{u}_r^{\mathrm{T}}\mathbf{F}}{\mathrm{j}\omega - \lambda_r}\mathbf{u}_r. \tag{3}$$

In order to obtain $\mathbf{u}_r$ and λ_r in Eq. (3), the following set of $2N$ equations shown in Eq. (4a) is solved. Here, $\mathbf{U}_r^{\dagger} = [\mathbf{U}_r, \lambda_r\mathbf{U}_r]^{\mathrm{T}}$ and λ_r are the generalized (complex) eigenvector and eigenvalue, respectively, at the rth mode of Eq. (4a). Further, $\mathbf{u}_r = \mathbf{U}_r/\sqrt{a_r}$ and $\mathbf{U}^{\dagger\mathrm{T}}\mathbf{A}\mathbf{U}^{\dagger} = \mathrm{diag}[a_r]$:

$$\lambda\mathbf{A}\boldsymbol{\chi} + \mathbf{B}\boldsymbol{\chi} = \mathbf{0}, \tag{4a}$$

where

$$\mathbf{A} = \begin{pmatrix} \mathbf{C} & \mathbf{M} \\ \mathbf{M} & \mathbf{0} \end{pmatrix}, \quad \mathbf{B} = \begin{pmatrix} \mathbf{K} & \mathbf{0} \\ \mathbf{0} & -\mathbf{M} \end{pmatrix} \quad \text{and} \quad \boldsymbol{\chi} = \begin{pmatrix} \mathbf{X} \\ \mathbf{V} \end{pmatrix}. \tag{4b}$$

The system parameters used in our studies are estimated from the measured response of experimental system of Fig. 2(b). The source and receiver sub-system parameters are first estimated by disconnecting all paths. Then, parameters of each path are individually determined, which is essentially the result of α scheme with the CM disconnect method. The estimated parameter set for the five and the two degrees-of-freedom systems is given in Table 1. The frequency range of interest is up to 300 Hz, and two to five distinct modes are considered depending on the system. Note that Eqs. (2) and (3) give identical responses and thus one could use either method for further calculations.

Table 1
Parameters of the five degrees-of-freedom system shown in Fig. 1

Stiffness elements k (N/mm)	$k_S = 27$, $k_R = 82$, $k_1 = 70$, $k_2 = 30$, $k_3 = 10$
Damping elements c (Ns/m)	$c_S = 0.62$, $c_R = 4.8$, $c_1 = 10$, $c_2 = 5$, $c_3 = 8$
Mass elements m (kg)	$m_S = 0.37$, $m_R = 0.37$, $m_1 = 0.15$, $m_2 = 0.10$, $m_3 = 0.07$
External force amplitude (N)	$F_S = 1$

The two degrees-of-freedom system of Fig. 2(a) is then obtained by assuming massless paths ($m_1 = m_2 = m_3 = 0$ kg).

3. Absolute and relative path measures in frequency domain

Many measures to quantify the parallel paths exist, as evident from the literature [2]. In order to categorize them, directional (absolute) measures of path are first introduced because they are useful for systems with only translational or rotational motions. Energy-based and relative measures are formulated next. All path measures are first presented and then applied to the five and the two degrees-of-freedom systems.

First, structural velocity amplitude (defined as $V(\omega) = \mathrm{j}\omega X(\omega)$) based measures are given. The translational mobility vector $\mathbf{Y}(\omega)$ given that the excitation is applied only at the source is given as: $\mathbf{Y} = \mathbf{V}/F_S = \mathrm{j}\omega\mathbf{Z}^{-1}(1,0,\ldots,0)^{\mathrm{T}}$. For example, the transfer mobility from source to receiver is $Y_R = V_R/F_S$. Likewise, the motion transmissibility (TR) from the source to the receiver is $\mathrm{TR}(\omega) = V_R/V_S$. Note that the motion transmissibility is usually defined in the direction of excitation force. Next, the interfacial force from source (or receiver) to path i is, respectively,

$$F_{iS}(\omega) = -\tilde{k}_{iS}(X_i - X_S) \quad \text{and} \quad F_{iR}(\omega) = -\tilde{k}_{iR}(X_i - X_R). \tag{5a,5b}$$

Eq. (5) may be called the direct method for the force estimation. Note that these forces include the contribution of dampers.

Next, when a vibrating system has both translational and rotational motions, use of a directional measure could give erroneous results because translational and rotational motions cannot be directly compared due to differences in units [2,3]. Therefore, energy-based measures [24,25,27,28] such as the power expressions that combine translational and rotational motions must be used. The time-averaged active power flow through a point is

$$\Pi(\omega) = \frac{1}{T}\int_0^T \mathrm{d}t\, \mathbf{v}^{\mathrm{T}}(t)\mathbf{f}(t) = \sum\nolimits_{q=x,y,z} \frac{1}{2} V_q F_q \cos(\varphi_{V_q} - \varphi_{F_q}) = \frac{1}{2}\mathrm{Re}\left[\mathbf{V}^{\mathrm{H}}(\omega)\mathbf{F}(\omega)\right],$$

where $\mathbf{v}(t) = \mathbf{V}(\omega)\mathrm{e}^{\mathrm{i}\omega t}$, $\mathbf{f}(t) = \mathbf{F}(\omega)\mathrm{e}^{\mathrm{i}\omega t}$, and the conjugate transpose is given by superscript H. This paper deals with only time-averaged powers and energies (in frequency domain). If these velocities and forces are evaluated for a whole system, this power yields the dissipation function of the system [29,30]. By using Eq. (1), the total active power is as follows:

$$\Pi_{\mathrm{Sys}} = \frac{1}{2}\mathrm{Re}[\mathbf{V}^H\mathbf{F}] = \frac{1}{2}\mathrm{Re}\left[\mathbf{V}^H\left(\tilde{\mathbf{K}} - \omega^2\mathbf{M}\right)\frac{\mathbf{V}}{\mathrm{j}\omega}\right] = \frac{1}{2}\mathbf{V}^H\mathbf{C}\mathbf{V} = \frac{1}{2}\mathrm{Re}[V_S^* F_S]. \tag{6}$$

where complex conjugate is denoted by superscript *, and the subscript "Sys" means the value for the whole system.

This formulation allows us to represent the dissipated power of the system by using only the velocity and force at the driving point because only the driving point term remains after taking the vector product $\mathbf{V}^H\mathbf{F}$. Note that Π is positive because non-null (real symmetric) $\mathbf{C}$ is positive definite ($\mathbf{V}^H\mathbf{C}\mathbf{V} > 0$). Similarly, the time-averaged energy flow for the whole system yields the mean (negative-valued) Lagrangian energy density L (in frequency domain) [27]:

$$\begin{aligned}\tfrac{1}{2}\mathrm{Re}[\mathbf{X}^H\mathbf{F}] &= \tfrac{1}{2}\mathrm{Re}[\mathbf{X}^H(\mathbf{K} + \mathrm{j}\omega\mathbf{C} - \omega^2\mathbf{M})\mathbf{X}] = \tfrac{1}{2}\mathbf{X}^H\mathbf{K}\mathbf{X} - \tfrac{1}{2}\mathbf{V}^H\mathbf{M}\mathbf{V},\\ &= \tfrac{1}{2}\mathrm{Re}\left[X_S^* F_S\right] = E_{k,\mathrm{Sys}} - E_{m,\mathrm{Sys}} = -L_{\mathrm{Sys}}(\mathbf{X},\mathbf{V},\omega).\end{aligned} \tag{7}$$

This is the difference between the kinetic (E_m) and potential (E_k) energies, which could be either positive or negative. For pure spring (k) or mass (m) elements, Eq. (7) would yield the time-averaged potential or kinetic energy terms as $E_{k,\mathrm{Sys}} = \mathbf{X}^H\mathbf{K}\mathbf{X}/2$, $E_{m,\mathrm{Sys}} = \mathbf{V}^H\mathbf{M}\mathbf{V}/2$, respectively. For instance, the averaged potential energy in the receiver-grounding path (the visco-elastic (c_R and k_R, or $\tilde{k}_R$) path in Figs. 1 and 2(a)) is $E_{k,\mathrm{Rg}} = -\mathrm{Re}[X_R^* F_{\mathrm{Rg}}]/2$, where the minus sign comes from the positive force definition. The time-averaged kinetic energy of a rigid body or mass element (B) is simply given from Ref. [28] as $E_{m,B} = m_B|V_B|^2/2$. This body may be receiver (R), source (S), or path i. Using Eq. (7), the time-averaged kinetic energy of path i (mass m_i) is obtained as $E_{m,i} = m_i|V_i|^2/2 = -\mathrm{Re}[X_i^* F_{iS}]/2 - \mathrm{Re}[X_i^* F_{iR}]/2$. The minus signs are due to the negative sign of the Lagrangian (L). Next, the total time-averaged energy of the system is given by the energy

function or Hamiltonian (in frequency domain) as

$$E_{k,\mathrm{Sys}} + E_{m,\mathrm{Sys}} = \mathbf{V}^H \frac{\partial L_{\mathrm{Sys}}}{\partial \mathbf{V}} - L_{\mathrm{Sys}} = \mathbf{V}^H \mathbf{M} \mathbf{V} + \frac{1}{2}\mathrm{Re}[X_S^* F_S]$$
$$= \frac{1}{2}\mathbf{P}^H \mathbf{M}^{-1} \mathbf{P} + \tfrac{1}{2}\mathbf{X}^H \mathbf{K} \mathbf{X} = H_{\mathrm{Sys}}(\mathbf{X}, \mathbf{P}, \omega). \tag{8}$$

Here, $\mathbf{P}(=\partial L/\partial \mathbf{V})$ is the generalized momentum vector. Note that only the driving point amplitudes, X_S (or V_S) and F_S, define the time-averaged dissipated power and Lagrangian energy in Eqs. (6) and (7) respectively. However, the total energy of Eq. (8) cannot be evaluated by driving point amplitudes alone.

Lastly, when path(s) are disconnected by either α or β scheme with one of the five disconnect methods as indicated in Fig. 3, the insertion loss (IL) concept may be utilized to characterize the ith path.

$$\mathrm{IL}_{\Xi} = 10 \log_{10} \langle \Xi^2_{\text{All Paths}} \rangle_t \Big/ \left\langle \Xi^2_{\alpha \text{ or } \beta \text{ Path } i} \right\rangle_t \text{(dB)}, \tag{9}$$

where Ξ is any computed measure of path i. Using this definition, a lower value of insertion loss in the α scheme or a higher value of insertion loss in the β scheme would suggest that the particular path is more dominant. When insertion loss assumes a negative value, the disconnected system should yield higher vibration level than the original system. High values of insertion loss should yield a clear path order since it is a relative measure. When the performance over a wide frequency range is desired, a spectral average of any path measure may be useful; $\Xi_{\mathrm{Ave}} = \sum_{\ell=1}^{N} |\Xi_\ell|/N$. Similarly, an averaged value of insertion loss is defined as

$$\mathrm{IL}_{\Xi,\mathrm{Ave}} = 10 \log_{10} \frac{1}{N} \sum_{\ell=1}^{N} \left\langle \Xi^2_{\text{All Paths, } \ell} \right\rangle_t \Big/ \left\langle \Xi^2_{\alpha \text{ or } \beta \text{ Path } i,\ell} \right\rangle_t.$$

Here, the average is taken before the logarithm, and the square is not taken for power/energy measures. Note that these spectral averages do not include any phase information. Alternately, averages may be found over octave or one-third octave bands with phase.

4. Estimation of interfacial path forces

4.1. Estimation using a computational method

In the first stage of the transfer path analysis, the path forces are indirectly estimated since the interfacial forces cannot be directly measured [8,19,20]. First, the frequency response functions (such as $\mathbf{H}_{P-R} = [\mathbf{X}/\mathbf{F}]_{P-R}$ or $H_{u,v} = X_u/F_v$) are measured without the source structure because the compliance type frequency response functions is found with free boundaries. The subscript P–R indicates a value measured for the path–receiver sub-system. Then the operational motion (response) vector ($\mathbf{X}$) is measured at the path locations with an operating source. The upper path forces F_{iS} transmitted through the parallel paths, under the operating conditions, are estimated as

$$\mathbf{F} = \mathbf{H}_{P-R}^{-1} \mathbf{X}. \tag{10}$$

By using the five degrees-of-freedom system of Fig. 1, a simulation is first performed. The upper path forces, F_{1S}, F_{2S} and F_{3S}, are estimated by using Eq. (10) and are shown in Fig. 4. The details of Eq. (10) will be given in the next sub-section. As is seen in Fig. 4, the resulting spectra are identical to the one given by the direct calculation of path forces as described by Eq. (5a) where the whole source–path–receiver system matrix and vector are employed to obtain the response vector $\mathbf{X}$. Fig. 4 shows three clear peaks, which are at the first (48.8 Hz), the third (138 Hz) and the fifth (244 Hz) modes. All motions participate in these three modes. Next, expand Eq. (10) for the ith path and express it in terms of contributions from the three paths:

$$F_{iS} = Z_{i,1} X_1 + Z_{i,2} X_2 + Z_{i,3} X_3, \quad i = 1, 2, 3. \tag{11}$$

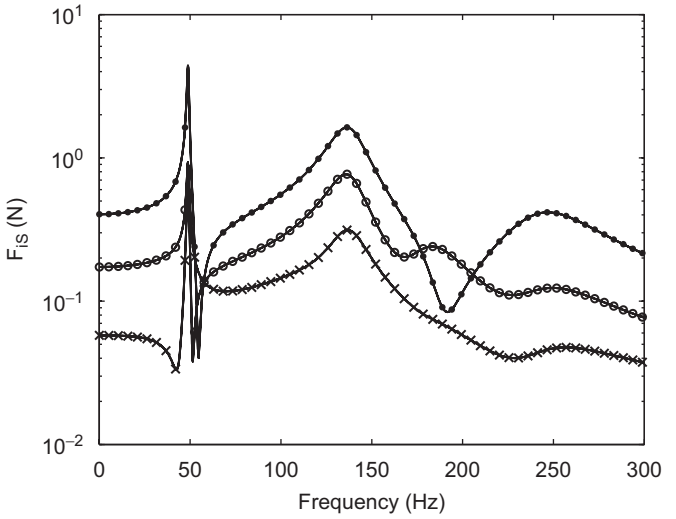

Fig. 4. Upper path force magnitude spectra estimated by direct and indirect methods (1 or 4). Key: —— (with ●), F_{1S} by Eq. (5a); ●, by Eq. (10) with method 1 or 4; —— (with ○), F_{2S} by Eq. (5a); ○, by Eq. (10) with method 1 or 4; —— (with x), F_{3S} by Eq. (5a); x, by Eq. (10) with Method 1 or 4.

Here, $Z_{m,n} = F_m/X_n$ are dynamic stiffness terms with blocked boundary conditions of the downward sub-system (explained in the next sub-section). Force spectra corresponding to these three terms in Eq. (11) are shown in Fig. 5. Observe that the contribution from Path i term is more dominant than the other two terms in the F_{iS} decomposition over lower and higher frequency regions.

4.2. Analytical determination of exact path forces

The upper path force F_{iS} may be obtained by the direct method (Eq. (5a)). However, the same force F_{iS} can be also obtained by using alternative analytical methods based on H or Z of the path–receiver sub-system. Four equivalent methods that exactly determine the path force F_{iS} are analytically described. For the sake of analytical simplicity, only two parallel paths (Path 1 and 2) in Fig. 1 are considered to form the four degrees-of-freedom system; Path 3 is completely removed.

In order to obtain the interfacial path force F_{iS} ($i = 1, 2$) of the four degrees-of-freedom source–path–receiver (S–P–R) system, the equations of motion for the path–receiver sub-system in Fig. 6(a) are considered. It is given by $\mathbf{F} = \mathbf{Z}_{P-R}\mathbf{X}$ or

$$\begin{pmatrix} F_{1S} \\ F_{2S} \\ 0 \end{pmatrix} = \begin{pmatrix} Z_{1,1} & Z_{1,2} & Z_{1,R} \\ Z_{2,1} & Z_{2,2} & Z_{2,R} \\ Z_{R,1} & Z_{R,2} & Z_{R,R} \end{pmatrix}_{P-R} \begin{pmatrix} X_1 \\ X_2 \\ X_R \end{pmatrix}, \tag{12}$$

where vectors $\mathbf{F}$ and $\mathbf{X}$ are operational responses for the whole source–path–receiver system. In order to obtain the path–receiver sub-system frequency response functions, $Z_{m,n}$ or $H_{u,v}$, the source structure (m_S and $\tilde{k}_S$) and the upper path springs and dampers ($\tilde{k}_{1S}$ and $\tilde{k}_{2S}$) must be removed. Then, Eq. (12) determines F_{1S} and F_{2S} exactly. Next, rewrite Eq. (12) by inverting the system matrix as: $\mathbf{X} = \mathbf{Z}_{P-R}^{-1}\mathbf{F} = \mathbf{H}_{P-R}\mathbf{F}$ or

$$\begin{pmatrix} X_1 \\ X_2 \\ X_R \end{pmatrix} = \begin{pmatrix} Z_{1,1} & Z_{1,2} & Z_{1,R} \\ Z_{2,1} & Z_{2,2} & Z_{2,R} \\ Z_{R,1} & Z_{R,2} & Z_{R,R} \end{pmatrix}_{P-R}^{-1} \begin{pmatrix} F_{1S} \\ F_{2S} \\ 0 \end{pmatrix} = \begin{pmatrix} H_{1,1} & H_{1,2} & H_{1,R} \\ H_{2,1} & H_{2,2} & H_{2,R} \\ H_{R,1} & H_{R,2} & H_{R,R} \end{pmatrix}_{P-R} \begin{pmatrix} F_{1S} \\ F_{2S} \\ 0 \end{pmatrix}. \tag{13}$$

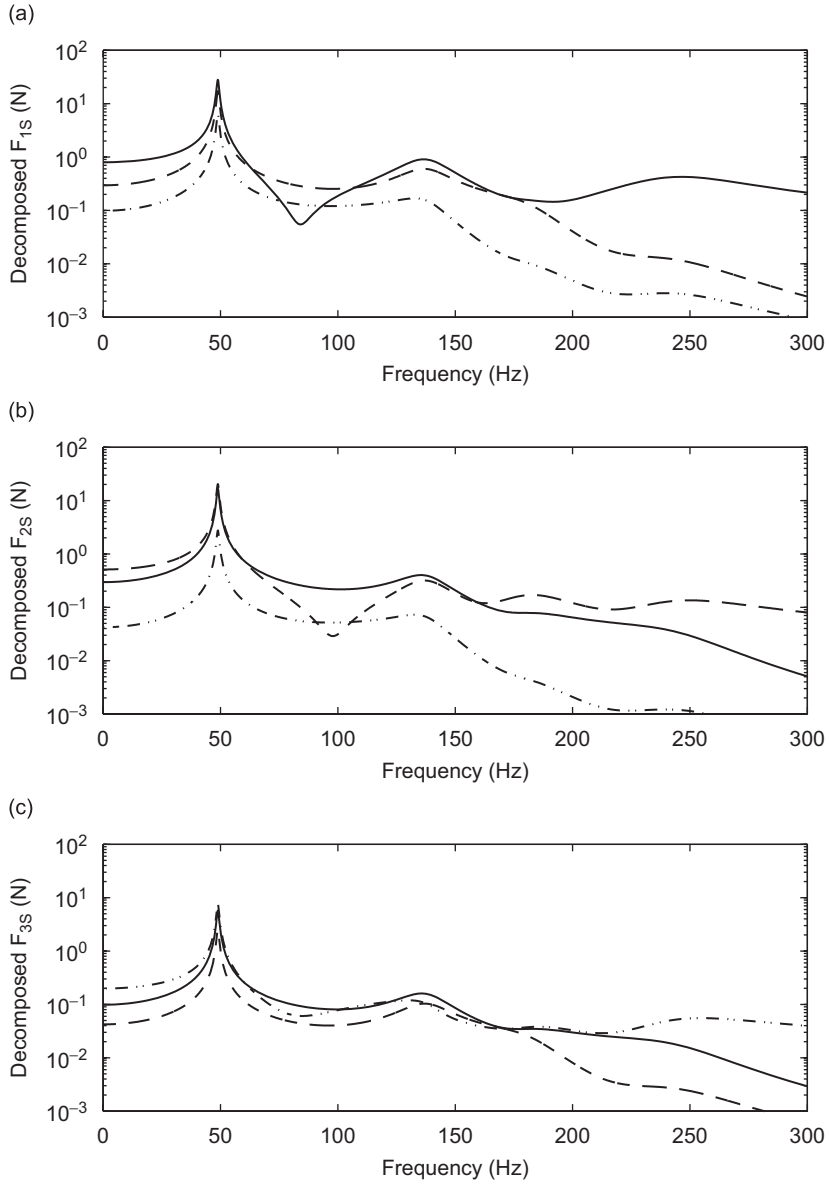

Fig. 5. Contribution of terms to upper path force F_{iS} spectra, where $i = 1, 2, 3$. (a) F_{1S} decomposition; (b) F_{2S} decomposition; (c) F_{3S} decomposition. Key: ——, Path 1 term; – – – –, Path 2 term; · – · – · –, Path 3 term.

Eq. (13) may be arranged only about the driving points (X_1, X_2) with the path forces (F_{1S}, F_{2S}). Accordingly, the path forces are then obtained as

$$\begin{pmatrix} F_{1S} \\ F_{2S} \end{pmatrix} = \begin{pmatrix} H_{1,1} & H_{1,2} \\ H_{2,1} & H_{2,2} \end{pmatrix}^{-1}_{P-R} \begin{pmatrix} X_1 \\ X_2 \end{pmatrix} \tag{14}$$

$$= \begin{pmatrix} Z'_{1,1} & Z'_{1,2} \\ Z'_{2,1} & Z'_{2,2} \end{pmatrix}_{P-R} \begin{pmatrix} X_1 \\ X_2 \end{pmatrix}. \tag{15}$$

Note that the $Z_{m,n}$ terms in Eqs. (13) and (15) are different (superscript dash is added to Eq. (15) for that reason), but that the $H_{u,v}$ terms in Eqs. (13) and (14) are the same. Although $Z \neq H^{-1}$ in general where Z and H

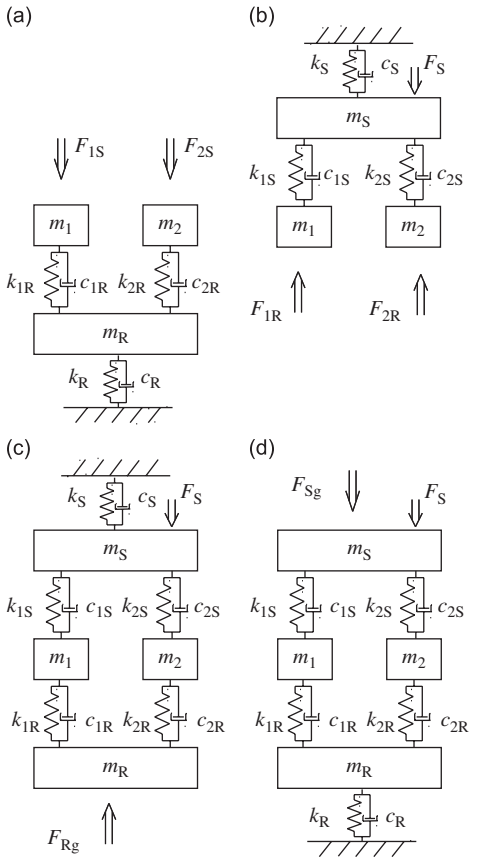

Fig. 6. Sub-systems of the four degrees-of-freedom system (obtained by completely removing Path 3 of Fig. 1). (a) Path–receiver sub-system; (b) source–path sub-system; (c) sub-system developed without grounding the receiver; (d) sub-system developed without grounding the source.

are scalar, the inverse relations of Eqs. (13)–(15) hold true. It is because these sets of equations uniquely determine the dynamics of the involved variables. Path forces in Eqs. (12) and (15) may be respectively expanded as

$$F_{iS} = Z_{i,1}\big|_{X_2=X_R=0} X_1 + Z_{i,2}\big|_{X_1=X_R=0} X_2 + Z_{i,R}\big|_{X_1=X_2=0} X_R \tag{16}$$

$$= Z_{i,1}\big|_{X_2=0} X_1 + Z_{i,2}\big|_{X_1=0} X_2, \quad i = 1 \text{ or } 2. \tag{17}$$

Here, the subscripts on the Z terms, which are replaced with superscript dash, indicate that the blocked boundary condition (BC) has to be imposed. The blocked condition is a virtual boundary for the stiffness type frequency response functions such as F/X, $F/\dot{X}$ and $F/\ddot{X}$. Observe a difference in the blocked boundary conditions in Eqs. (16) and (17), due to different equations used. If the stiffness (Z) type frequency response functions are available, the estimation process should be simpler since the matrix inversion will no longer be required. However, it is difficult to apply the blocked boundary conditions in experimental work. Conversely, the free boundary conditions, which are employed by the compliance (H) type frequency response functions such as X/F, $\dot{X}/F$ and $\ddot{X}/F$, are easy to implement, though some additional calculations and measurements are required. Overall, the following four path force estimation methods, which should yield the exact path force, are classified in terms of the frequency response function matrix employed. *Method* 1: Apply the direct method with the stiffness (Z) type frequency response functions given blocked boundary conditions for the all points of the path–receiver sub-system using Eq. (12) or (16). *Method* 2: Apply the inversion method with the compliance (H) type frequency response functions given free boundary conditions for the all points of the

path–receiver sub-system using Eq. (13) ($\mathbf{F} = \mathbf{H}_{P-R}^{-1}\mathbf{X}$). *Method* 3: Apply the direct method with the stiffness type frequency response functions given blocked boundary conditions only for the driving points of the path–receiver sub-system using Eq. (15) or (17). *Method* 4: Apply the inversion method with the compliance type frequency response functions given free boundary conditions only for driving points of the path–receiver sub-system using Eq. (14). This method is most widely used in practice [8,12,14–16]. The direct path force is first analytically obtained by using Eq. (5a). Analytical details of the competing four methods are then given, and some equivalence is also shown. Finally, the blocked boundary condition type frequency response functions is derived to discuss its utility.

4.3. Closed form solution for path forces

The equations of motion (1) for the four degrees-of-freedom system (with only Path 1 and 2) are given by $\mathbf{F} = \mathbf{Z}\mathbf{X}$, where $\mathbf{F} = (F_S, 0, 0, 0)^{\mathrm{T}}$, $\mathbf{X} = (X_S, X_1, X_2, X_R)^{\mathrm{T}}$, $\mathbf{M} = \mathrm{diag}(m_S, m_1, m_2, m_R)$, and

$$\tilde{\mathbf{K}} = \begin{pmatrix} \tilde{k}_{1S} + \tilde{k}_{2S} + \tilde{k}_S & -\tilde{k}_{1S} & -\tilde{k}_{2S} & 0 \\ -\tilde{k}_{1S} & \tilde{k}_{1S} + \tilde{k}_{1R} & 0 & -\tilde{k}_{1R} \\ -\tilde{k}_{2S} & 0 & \tilde{k}_{2S} + \tilde{k}_{2R} & -\tilde{k}_{2R} \\ 0 & -\tilde{k}_{1R} & -\tilde{k}_{2R} & \tilde{k}_{1R} + \tilde{k}_{2R} + \tilde{k}_R \end{pmatrix}. \tag{18}$$

The harmonic response amplitude vector $\mathbf{X}$ is obtained as: $\mathbf{X} = \mathbf{Z}^{-1}\mathbf{F} = \mathbf{H}\mathbf{F}$. A closed form solution for this case, in terms of X_S, X_1, X_2 and X_R, is given as follows:

$$\begin{aligned} X_S = \frac{F_S}{\det \mathbf{Z}} \big[& -m_1 m_2 m_R \omega^6 + \big\{ \big(m_1 \tilde{k}_2 + m_2 \tilde{k}_1\big) m_R + m_1 m_2 \tilde{k}_b \big\} \omega^4 \\ & - \big\{ m_1 \big(\big(\tilde{k}_{1R} + \tilde{k}_R\big) \tilde{k}_{2R} + \tilde{k}_{2S} \tilde{k}_b \big) + m_2 \big(\big(\tilde{k}_{2R} + \tilde{k}_R\big) \tilde{k}_{1R} + \tilde{k}_{1S} \tilde{k}_b \big) \\ & + m_R \tilde{k}_1 \tilde{k}_2 \big\} \omega^2 + \tilde{k}_a + \tilde{k}_R \tilde{k}_1 \tilde{k}_2 \big], \end{aligned} \tag{19a}$$

$$X_1 = \frac{F_S}{\det \mathbf{Z}} \big[\tilde{k}_{1S} \big\{ m_2 m_R \omega^4 - \big(m_R \tilde{k}_2 + m_2 \tilde{k}_b\big) \omega^2 + \tilde{k}_R \tilde{k}_2 \big\} + \tilde{k}_a \big], \tag{19b}$$

$$X_2 = \frac{F_S}{\det \mathbf{Z}} \big[\tilde{k}_{2S} \big\{ m_1 m_R \omega^4 - \big(m_R \tilde{k}_1 + m_1 \tilde{k}_b\big) \omega^2 + \tilde{k}_R \tilde{k}_1 \big\} + \tilde{k}_a \big], \tag{19c}$$

$$X_R = \frac{F_S}{\det \mathbf{Z}} \big[-\big(m_1 \tilde{k}_{2S} \tilde{k}_{2R} + m_2 \tilde{k}_{1S} \tilde{k}_{1R}\big) \omega^2 + \tilde{k}_a \big]. \tag{19d}$$

Here, $\det \mathbf{Z}$ is the determinant of $\mathbf{Z}$, and the followings symbols are defined for the sake of brevity; $\tilde{k}_1 = \tilde{k}_{1S} + \tilde{k}_{1R}$, $\tilde{k}_2 = \tilde{k}_{2S} + \tilde{k}_{2R}$, $\tilde{k}_a = \tilde{k}_{1S} \tilde{k}_{1R} \tilde{k}_2 + \tilde{k}_{2S} \tilde{k}_{2R} \tilde{k}_1$ and $\tilde{k}_b = \tilde{k}_{1R} + \tilde{k}_{2R} + \tilde{k}_R$. Next, expressions for the (direct) path forces are obtained from Eq. (5a) as

$$\begin{aligned} F_{1S} = \frac{F_S \tilde{k}_{1S}}{\det \mathbf{Z}} \big[& -m_1 m_2 m_R \omega^6 - \big\{ m_1 m_R \tilde{k}_2 + m_1 m_2 \tilde{k}_b + m_2 m_R \tilde{k}_{1R} \big\} \omega^4 \\ & - \big\{ \tilde{k}_2 \big(m_1 \big(\tilde{k}_{1R} + \tilde{k}_R\big) + m_R \tilde{k}_{1R} \big) + m_2 \tilde{k}_{1R} \big(\tilde{k}_{2R} + \tilde{k}_R\big) + m_1 \tilde{k}_{2S} \tilde{k}_{2R} \big\} \omega^2 + \tilde{k}_{1R} \tilde{k}_R \tilde{k}_2 \big], \end{aligned} \tag{20a}$$

$$\begin{aligned} F_{2S} = \frac{F_S \tilde{k}_{2S}}{\det \mathbf{Z}} \big[& -m_1 m_2 m_R \omega^6 - \big\{ m_2 m_R \tilde{k}_1 + m_1 m_2 \tilde{k}_b + m_1 m_R \tilde{k}_{2R} \big\} \omega^4 \\ & - \big\{ \tilde{k}_1 \big(m_2 \big(\tilde{k}_{2R} + \tilde{k}_R\big) + m_R \tilde{k}_{2R} \big) + m_1 \tilde{k}_{2R} \big(\tilde{k}_{1R} + \tilde{k}_R\big) + m_2 \tilde{k}_{1S} \tilde{k}_{1R} \big\} \omega^2 + \tilde{k}_{2R} \tilde{k}_R \tilde{k}_1 \big]. \end{aligned} \tag{20b}$$

4.4. Indirect force estimation using Method 1 or 3 with blocked boundaries

The dynamic stiffness matrix of Eq. (12) for Method 1 may be easily obtained by writing all equations for the path–receiver sub-system. Another way would be to apply the blocked boundary conditions, and this

method should be easier because only one mass could move under this blocked boundary conditions. For instance, in order to find $Z_{1,1}|_{X_2=X_R=0}$, block m_2 and m_R ($X_2 = X_R = 0$), and the governing equation for m_1 gives $Z_{1,1}|_{X_2=X_R=0} = \tilde{k}_{1R} - \omega^2 m_1$. When m_1 and m_R are blocked ($X_1 = X_R = 0$), $Z_{1,2}|_{X_1=X_R=0} = 0$ because no force is transmitted to m_1. Other elements are obtained in the same manner. Note that $\mathbf{Z}$ is a symmetric matrix. The resulting dynamic stiffness matrix for the four degrees-of-freedom system is

$$\mathbf{Z}_{P-R} = \begin{pmatrix} \tilde{k}_{1R} - \omega^2 m_1 & 0 & -\tilde{k}_{1R} \\ 0 & \tilde{k}_{2R} - \omega^2 m_2 & -\tilde{k}_{2R} \\ -\tilde{k}_{1R} & -\tilde{k}_{2R} & \tilde{k}_b - \omega^2 m_R \end{pmatrix}. \tag{21}$$

The upper path force F_{iS} is obtained by Method 1 using Eqs. (12), (19) and (21). Method 1 matches well with the direct method (20), which can be analytically proven. Thus,

$$F_{iS} = -\tilde{k}_{iS}(X_i - X_S) = Z_{i,1}|_{X_2=X_R=0} X_1 + Z_{i,2}|_{X_1=X_R=0} X_2 + Z_{i,R}|_{X_1=X_2=0} X_R. \tag{22}$$

Here, $i = 1$ or 2 for the four degrees-of-freedom system, but the above procedure can handle any number of parallel paths.

We next employ Method 3 for Eq. (15) or (17) with another blocked boundary. Although the $\mathbf{Z}$ matrix is smaller, more analytical calculations are required since two masses could move, and then both equations have to be simultaneously solved. First, block m_2 ($X_2 = 0$) and solve the equations for m_1 and m_R. Next, block m_1 ($X_1 = 0$) and similarly solve the equations for m_2 and m_R. Then,

$$\begin{pmatrix} X_1 \\ X_R \end{pmatrix} = \begin{pmatrix} \tilde{k}_{1R} - \omega^2 m_1 & -\tilde{k}_{1R} \\ -\tilde{k}_{1R} & \tilde{k}_b - \omega^2 m_R \end{pmatrix}^{-1} \begin{pmatrix} F_1 \\ 0 \end{pmatrix}, \quad \begin{pmatrix} X_2 \\ X_R \end{pmatrix} = \begin{pmatrix} \tilde{k}_{2R} - \omega^2 m_2 & -\tilde{k}_{2R} \\ -\tilde{k}_{2R} & \tilde{k}_b - \omega^2 m_R \end{pmatrix}^{-1} \begin{pmatrix} F_2 \\ 0 \end{pmatrix}. \tag{23}$$

Eq. (23) gives the following elements of $\mathbf{Z}$: $Z_{1,1}|_{X_2=0} = \det \mathbf{Z}_{X_2=0} / (\tilde{k}_b - \omega^2 m_R)$ and $Z_{2,2}|_{X_1=0} = \det \mathbf{Z}_{X_1=0} / (\tilde{k}_b - \omega^2 m_R)$. Here, $\det \mathbf{Z}_{X_1=0} = m_2 m_R \omega^4 - (m_R \tilde{k}_{2R} + m_2 \tilde{k}_b)\omega^2 + \tilde{k}_{2R}(\tilde{k}_{1R} + \tilde{k}_R)$ and $\det \mathbf{Z}_{X_2=0} = m_1 m_R \omega^4 - (m_R \tilde{k}_{1R} + m_1 \tilde{k}_b)\omega^2 + \tilde{k}_{1R}(\tilde{k}_{2R} + \tilde{k}_R)$. The off-diagonal terms are obtained from the force balance equations. For instance, $F_2 = -\tilde{k}_{2R} X_R$ under $X_2 = 0$ gives $Z_{2,1}|_{X_2=0}$, which is equal to $Z_{1,2}|_{X_1=0}$ because of the symmetric property of $\mathbf{Z}$; $Z_{2,1}|_{X_2=0} = -\tilde{k}_{1R}\tilde{k}_{2R} / (\tilde{k}_b - \omega^2 m_R) = Z_{1,2}|_{X_1=0}$. Thus, $\mathbf{Z}$ of Eq. (15) is obtained as follows:

$$\mathbf{Z}'_{P-R} = \begin{pmatrix} Z'_{1,1} & Z'_{1,2} \\ Z'_{2,1} & Z'_{2,2} \end{pmatrix}_{P-R} = \frac{1}{\tilde{k}_b - \omega^2 m_R} \begin{pmatrix} \det \mathbf{Z}_{X_2=0} & -\tilde{k}_{1R}\tilde{k}_{2R} \\ -\tilde{k}_{1R}\tilde{k}_{2R} & \det \mathbf{Z}_{X_1=0} \end{pmatrix} \equiv \mathbf{Z}_{\mathrm{Dr}}. \tag{24}$$

From Eq. (17), F_{1S} is given as

$$F_{1S} = Z_{1,1}|_{X_2=0} X_1 + Z_{1,2}|_{X_1=0} X_2 = \frac{\det \mathbf{Z}_{X_2=0}}{\tilde{k}_b - \omega^2 m_R} X_1 - \frac{\tilde{k}_{1R}\tilde{k}_{2R}}{\tilde{k}_b - \omega^2 m_R} X_2. \tag{25}$$

By substituting Eq. (19) into Eq. (25), we have analytically proven that Eq. (25) yields the same force as Eq. (20a). Likewise, the force F_{2S} can be verified.

4.5. Indirect estimation using Methods 2 and 4 with free boundaries

Method 2 can be easily proven without obtaining all of the $H_{u,v}$ terms. First, apply F_1 on m_1 in the path–receiver sub-system with the free boundary condition. Next, apply F_2 on m_2, and lastly apply F_R on m_R to obtain the elements of compliance vectors as $(X_1, X_2, X_R)^{\mathrm{T}} / F_1 = \mathbf{Z}^{-1}_{P-R}(1,0,0)^{\mathrm{T}}$, $(X_1, X_2, X_R)^{\mathrm{T}} / F_2 = \mathbf{Z}^{-1}_{P-R}(0,1,0)^{\mathrm{T}}$, and $(X_1, X_2, X_R)^{\mathrm{T}} / F_3 = \mathbf{Z}^{-1}_{P-R}(0,0,1)^{\mathrm{T}}$. These three equations may be combined to yield $\mathbf{H}_{P-R} = \mathbf{Z}^{-1}_{P-R}$. The inverse relation can be seen in Eq. (13).

By calculating the matrix inversion $\mathbf{Z}_{P\text{-}R}^{-1}$ of Eq. (21), Method 4 may be analytically formulated. Since $H_{u,v}$ terms in Eqs. (13) and (14) are the same, $\mathbf{H}$ matrix in Eq. (14) is constructed as follows:

$$\mathbf{H}_{\mathrm{Dr}} \equiv \begin{pmatrix} H_{1,1} & H_{2,1} \\ H_{2,1} & H_{2,2} \end{pmatrix} = \frac{1}{\det \mathbf{Z}_{P-R}} \begin{pmatrix} H_{1,1}^{\mathrm{Num}} & \tilde{k}_{1R}\tilde{k}_{2R} \\ \tilde{k}_{1R}\tilde{k}_{2R} & H_{2,2}^{\mathrm{Num}} \end{pmatrix}, \tag{26a}$$

$$H_{1,1}^{\mathrm{Num}} = m_2 m_R \omega^4 - \left(m_R \tilde{k}_{2R} + m_2 \tilde{k}_b\right)\omega^2 + \tilde{k}_{2R}\left(\tilde{k}_{1R} + \tilde{k}_R\right), \tag{26b}$$

$$H_{2,2}^{\mathrm{Num}} = m_1 m_R \omega^4 - \left(m_R \tilde{k}_{1R} + m_1 \tilde{k}_b\right)\omega^2 + \tilde{k}_{1R}\left(\tilde{k}_{2R} + \tilde{k}_R\right), \tag{26c}$$

$$\begin{aligned} \det \mathbf{Z}_{P-R} = & -m_1 m_2 m_R \omega^6 + \left\{m_1 m_2 \tilde{k}_b + m_R\left(m_1 \tilde{k}_{2R} + m_2 \tilde{k}_{1R}\right)\right\}\omega^4 \\ & - \left\{m_1 \tilde{k}_{2R}\left(\tilde{k}_{1R} + \tilde{k}_R\right) + m_2 \tilde{k}_{1R}\left(\tilde{k}_{2R} + \tilde{k}_R\right) - m_R \tilde{k}_{1R}\tilde{k}_{2R}\right\}\omega^2 + \tilde{k}_{1R}\tilde{k}_{2R}\tilde{k}_R. \end{aligned} \tag{26d}$$

The subscript Dr in Eq. (26a) indicates that the frequency response function matrix is found only at the driving points. By further calculating the matrix inversion of Eq. (26), it can be shown that $\mathbf{H}_{\mathrm{Dr}}^{-1} = \mathbf{Z}_{\mathrm{Dr}}$. In summary, the four methods yield exactly the same path forces. Fig. 4 compares direct (5a) and indirect Methods 1 and 4 for the five degrees-of-freedom system with 3 paths. Of the four methods described above, Method 1 is analytically the easiest, but experimentally most difficult because of the blocked boundary conditions. Furthermore, in finite element solutions, determination of $H_{u,v}$ or $Z_{m,n}$ terms for all field points (nodes) might be unrealistic. On the other hand, Method 4 is the easiest to implement and thus commonly used in practice.

4.6. Determination of other interfacial forces

The interfacial forces in lower paths and source or receiver-grounding paths can be obtained in a similar manner. First, the exact lower path forces, F_{1R} and F_{2R}, of the four degrees-of-freedom system are obtained by considering the source–path (S–P) sub-system of Fig. 6(b). The equations for the source–path sub-system are given by $\mathbf{F} = \mathbf{Z}_{S-P}\mathbf{X}$, or

$$\begin{pmatrix} F_S \\ F_{1R} \\ F_{2R} \end{pmatrix} = \begin{pmatrix} Z_{S,S} & Z_{S,1} & Z_{S,2} \\ Z_{1,S} & Z_{1,1} & Z_{1,2} \\ Z_{2,S} & Z_{2,1} & Z_{2,2} \end{pmatrix}_{S-P} \begin{pmatrix} X_S \\ X_1 \\ X_2 \end{pmatrix}, \tag{27}$$

where $\mathbf{F}$ and $\mathbf{X}$ are the operational responses of the whole source–path–receiver system, and the Z terms are obtained for the source–path sub-system. Eqs. (14) and (27) indicate that more frequency response functions are needed to obtain the lower path force F_{iR} than the upper path force F_{iS}.

$$F_{iR} = Z_{i,S}\big|_{X_1=X_2=0} X_S + Z_{i,1}\big|_{X_S=X_2=0} X_1 + Z_{i,2}\big|_{X_S=X_1=0} X_2 \quad i = 1 \text{ or } 2. \tag{28}$$

As a computational result, Fig. 7(a) compares the 3 path spectra for the five degrees-of-freedom system. Again, the direct force F_{iR} by Eq. (5b) completely agrees with the estimated F_{iR} by Eq. (28); it can be analytically proven in a similar manner. Further, the F_{iR} spectra show similar trends (except around 190 Hz) with the F_{iS} spectra in Fig. 4. On the other hand, the driving point estimation as expressed below by Eq. (29) differs, since the frequency response functions about F_S are missing:

$$\begin{pmatrix} F_{1R} \\ F_{2R} \end{pmatrix} \sim \begin{pmatrix} H_{1,1} & H_{1,2} \\ H_{2,1} & H_{2,2} \end{pmatrix}_{S-P}^{-1} \begin{pmatrix} X_1 \\ X_2 \end{pmatrix}. \tag{29}$$

Here, the matrix inverse in Eq. (29) produces pseudo (non-exact) dynamic stiffness Z.

Next, in order to estimate the transmitted force F_{Rg} to the receiver from the receiver-grounding path, the path spring and damper ($\tilde{k}_R$) are removed or disconnected from the system, as shown in Fig. 6(c).

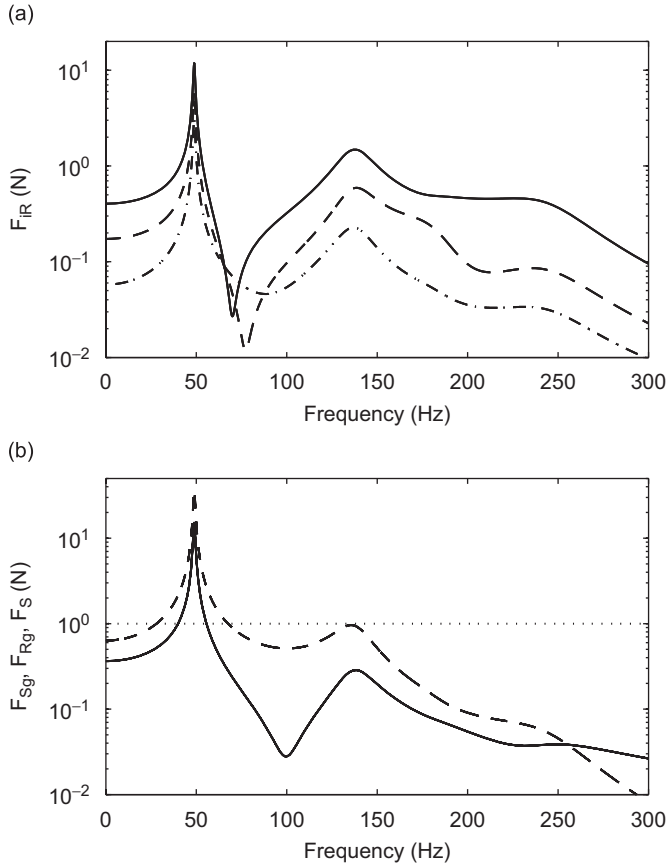

Fig. 7. Interfacial and transmitted force spectra. (a) Downward path forces F_{iR}; (b) forces transmitted by the source (F_{Sg}) and receiver (F_{Rg}) sub-systems into the ground. Key: (a) ——, F_{Rg}; – – – –, F_{2R}; – · – · –, F_{3R}. (b) ——, F_{Sg}; – – – –, F_{Rg}, · · · · ·, F_S. Both direct and indirect methods yield the same results. (Each line represents 2 lines corresponding to direct and indirect methods.)

The equation for this sub-system is $\mathbf{F} = \mathbf{Z}_{w/o\ kR}\mathbf{X}$ or $\left(F_S, 0, 0, F_{\mathrm{Rg}}\right)^{\mathrm{T}} = \mathbf{Z}_{w/o\ kR}(X_S, X_1, X_2, X_R)^{\mathrm{T}}$. This yields the indirect exact force F_{Rg} as the summation of the 4 terms. However, by taking an inverse of $\mathbf{Z}_{w/o\ kR}$, forces F_{Rg} and F_S are estimated as

$$\begin{pmatrix} F_S \\ F_{\mathrm{Rg}} \end{pmatrix} = \begin{pmatrix} H_{S,S} & H_{S,R} \\ H_{R,S} & H_{R,R} \end{pmatrix}^{-1} \begin{pmatrix} X_S \\ X_R \end{pmatrix} = \begin{pmatrix} Z'_{S,S} & Z'_{S,R} \\ Z'_{R,S} & Z'_{R,R} \end{pmatrix} \begin{pmatrix} X_S \\ X_R \end{pmatrix}, \tag{30}$$

where the dash indicates different blocked boundary conditions. Eq. (30) gives yet another form of the exact force F_{Rg}:

$$F_{\mathrm{Rg}} = Z_{R,S}\big|_{X_R=0} X_S + Z_{R,R}\big|_{X_S=0} X_R. \tag{31}$$

Fig. 7(b) confirms the equivalence of F_{Rg} estimated by $F_{\mathrm{Rg}} = -\tilde{k}_R X_R$ (direct method) and Eq. (31) for the five degrees-of-freedom system.

Lastly, in order to determine the transmitted force F_{Sg} from the source to the ground, the source spring and damper ($\tilde{k}_S$) are removed from the original system, as shown in Fig. 6(d). The equation for this sub-system is $\mathbf{F} = \mathbf{Z}_{w/o\ kS}\mathbf{X}$ or $(F_S + F_{\mathrm{Sg}}, 0, 0, 0)^{\mathrm{T}} = \mathbf{Z}_{w/o\ kS}(X_S, X_1, X_2, X_R)^{\mathrm{T}}$. This equation gives F_{Sg} as a summation of four terms minus the excitation force F_S. Similarly, by taking an inverse of $\mathbf{Z}_{w/o\ kS}$, a simplified form is obtained as

$$F_{\mathrm{Sg}} = H^{-1}_{S,S} X_S - F_S = H^{-1}_{S,1} X_1 - F_S = H^{-1}_{S,2} X_2 - F_S = H^{-1}_{S,R} X_R - F_S. \tag{32}$$

Table 2
Summary of the impedance terms required for the exact determination of interfacial forces for the four degrees-of-freedom system (with Path 1 and 2)

Interfacial force	Minimum impedance terms required	
	With blocked BC	With free BC
F_{iS}	$Z_{i,1}\big\vert_{X_2=0}$ and $Z_{i,2}\big\vert_{X_1=0}$	$\begin{pmatrix} H_{1,1} & H_{1,2} \\ H_{2,1} & H_{2,2} \end{pmatrix}$
F_{iR}	$Z_{i,S}\big\vert_{X_1=X_2=0}, Z_{i,1}\big\vert_{X_S=X_2=0}$ and $Z_{i,2}\big\vert_{X_S=X_1=0}$	$\begin{pmatrix} H_{S,S} & H_{S,1} & H_{S,2} \\ H_{1,S} & H_{1,1} & H_{1,2} \\ H_{2,S} & H_{2,1} & H_{2,2} \end{pmatrix}$
F_{Sg}	$Z_{S,S}, Z_{S,1}, Z_{S,2}$ or $Z_{S,R}$*	$H_{S,S}, H_{S,1}, H_{S,2}$ or $H_{S,R}$
F_{Rg}	$Z_{R,S}\big\vert_{X_R=0}$ and $Z_{R,R}\big\vert_{X_S=0}$	$\begin{pmatrix} H_{S,S} & H_{S,R} \\ H_{R,S} & H_{R,R} \end{pmatrix}$

Here, * denotes without blocked boundary condition.

Here, a scalar inverse relationship $H_{S,i}^{-1} = Z_{i,S}\big\vert_{N/A}$ ($i = S$, 1, 2 or R) may be defined, where the subscript N/A means "no blocked boundary conditions". The first equation in Eq. (32) is

$$\frac{X_S}{F_S + F_{\mathrm{Sg}}} = \left(\frac{X_S}{F_S}\right). \tag{33}$$

The right-hand side of Eq. (33) is dynamic compliance of the sub-system in Fig. 6(d) where F_S is the applied force of any amplitude (as long as the system is linear) and X_S is the response [31]. In Eq. (33), F_{Sg} is the source to ground path force (defined by $\tilde{k}_S$) of the original system, and X_S is the response to F_S. Fig. 7(b) shows that the direct force obtained by using $F_{\mathrm{Sg}} = -\tilde{k}_S X_S$ matches well with the F_{Sg} estimated by Eq. (32) for the five degrees-of-freedom system. Also, the peaks around 244 Hz (Path 1 mode) disappear in Fig. 7(b). Finally, Table 2 summarizes the minimum terms of $H_{u,v}$ and $Z_{m,n}$ that are needed to estimate interfacial forces.

5. Energy flow in the parallel path system

The time-averaged active power and energy expressions are applied to the five degrees-of-freedom system of Fig. 1. Recall that the total dissipated power and the Lagrangian energy of the system can be estimated by using only the driving point velocity and force as given by Eqs. (6) and (7) respectively. The interfacial forces determined by using direct or indirect methods are used for calculations. The same driving point concept is now applied to all sub-systems: the source (m_S and $\tilde{k}_S$), the three separate paths (each with m_i, $\tilde{k}_{iS}$ and $\tilde{k}_{iR}$), and the receiver (m_R and $\tilde{k}_R$).

To start with, the dissipated power and the Lagrangian energy in the ith path are

$$\Pi_i = \frac{1}{2}\mathrm{Re}[V_S^* F_{iS}] + \frac{1}{2}\mathrm{Re}[V_R^* F_{iR}], \quad L_i = -\frac{1}{2}\mathrm{Re}[X_S^* F_{iS}] - \frac{1}{2}\mathrm{Re}[X_R^* F_{iR}]. \tag{34a, 34b}$$

Note that the sign of each term depends on the definition of positive force. The driving points for the ith path sub-system are the source–path and path–receiver connection points. The power Π_i spectra are plotted in Fig. 8. Observe that the power spectra assume only positive values at all frequencies [13]. The total dissipated power and Lagrangian energy within all of the paths are given by $\Pi_P = \sum_{i=1}^{3}\Pi_i$ and $L_P = \sum_{i=1}^{3} L_i$, respectively. Likewise, the dissipated power in upper and lower paths may be obtained by separately considering $\tilde{k}_{iS}$ and $\tilde{k}_{iR}$ elements whose sum also gives Π_i. However, to obtain L_i in this manner, the kinetic energy within the path has to be considered as well. Secondly, the dissipated power within the receiver is

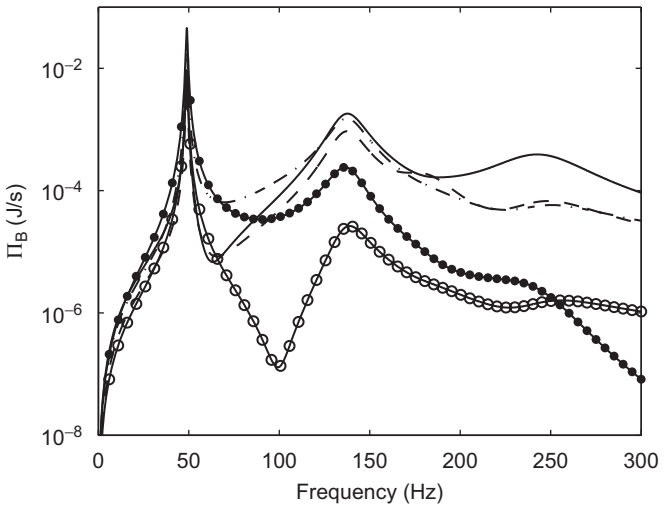

Fig. 8. Dissipated power spectra for all sub-systems. Key: ——, Π_1 by Eq. (34a); – – – –, Π_2 by Eq. (34a); · – · – · –, Π_3 by Eq. (34a); —— (with ●), Π_R by Eq. (35a); ●, Π_{Rg} by Eq. (35b); —— (with o), Π_S by Eq. (37a); o, Π_{Sg} by Eq. (37b).

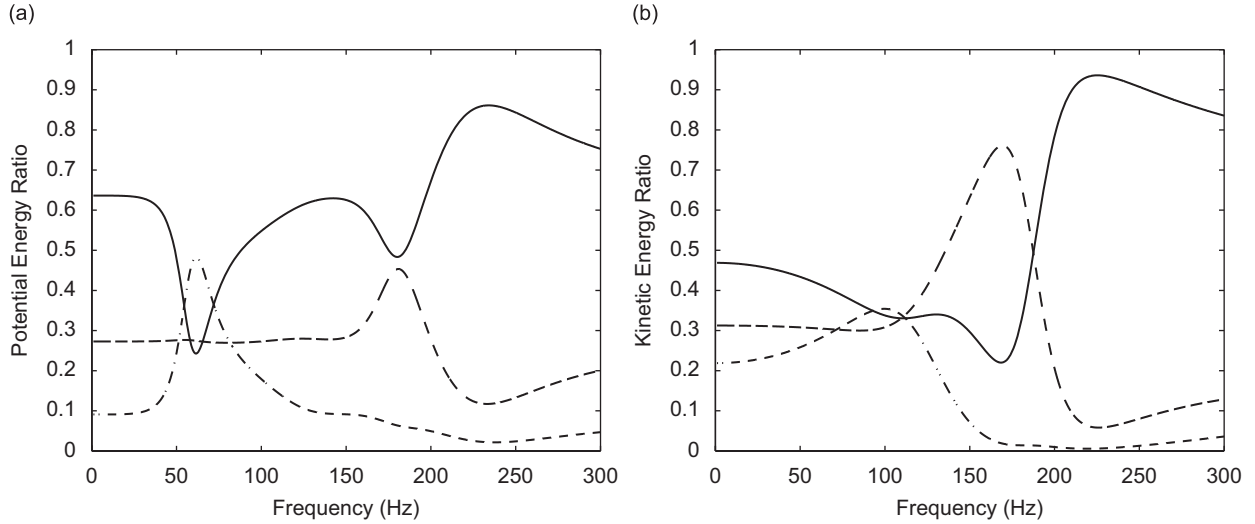

Fig. 9. Potential and kinetic energy spectra. (a) Potential energy ratios for all paths; (b) kinetic energy ratios for all paths. Key: (a) ——, $E_{k,1}/E_{k,P}$; – – – –, $E_{k,2}/E_{k,P}$; · – · – · –, $E_{k,3}/E_{k,P}$. (b) ——, $E_{m,1}/E_{m,P}$; – – – –, $E_{m,2}/E_{m,P}$; · – · – · –, $E_{m,3}/E_{m,P}$.

obtained by considering only the driving points for the sub-system.

$$\Pi_R = -\sum_{i=1}^{3} \frac{1}{2}\mathrm{Re}[V_R^* F_{iR}], \quad \Pi_{\mathrm{Rg}} = -\frac{1}{2}\mathrm{Re}[V_R^* F_{\mathrm{Rg}}] \tag{35a, 35b}$$

Since the mass m_R does not dissipate any energy, the dissipated power in the receiver sub-system and in the receiver-grounding path (given by $\tilde{k}_R$) are the same. Thus, $\Pi_R = \Pi_{\mathrm{Rg}}$. The results shown in Fig. 8 confirm, computationally, the above because identical spectra are found. Also, observe that the path sub-systems dissipate more powers than the source or receiver sub-system beyond 100 Hz. On the other hand, the Lagrangian energy expression includes the kinetic energy of the receiver mass m_R:

$$L_R = \sum_{i=1}^{3} \frac{1}{2}\mathrm{Re}[X_R^* F_{iR}] = \frac{1}{2} m_R |V_R|^2 + \frac{1}{2}\mathrm{Re}[X_R^* F_{\mathrm{Rg}}]. \tag{36}$$

Thirdly, the dissipated power and the Lagrangian energy within the source are:

$$\Pi_S = \Pi_{\mathrm{Sys}} - \sum_{i=1}^{3} \frac{1}{2}\mathrm{Re}[V_S^* F_{iS}], \quad \Pi_{Sg} = -\frac{1}{2}\mathrm{Re}[V_S^* F_{\mathrm{Sg}}], \tag{37a, 37b}$$

$$L_S = L_{\mathrm{Sys}} + \sum_{i=1}^{3} \frac{1}{2}\mathrm{Re}[X_S^* F_{iS}] = \frac{1}{2} m_S |V_S|^2 + \frac{1}{2}\mathrm{Re}[X_S^* F_{\mathrm{Sg}}]. \tag{38}$$

Again, since the source mass m_R does not dissipate energy, the active power dissipated in the source grounding path gives the same value. However, the Lagrangian energy to the source sub-system is expressed by subtracting the potential energy of the grounding path from the kinetic energy of the source mass.

Here, the total dissipated power and the Lagrangian energy of the entire system are:

$$\Pi_{\mathrm{Sys}} = \frac{1}{2}\mathrm{Re}[V_S^* F_S] = \Pi_S + \Pi_P + \Pi_R, \quad L_{\mathrm{Sys}} = -\frac{1}{2}\mathrm{Re}[X_S^* F_S] = L_S + L_P + L_R \tag{39a, 39b}$$

Recall that the Lagrangian energy defined by Eq. (7) assumes both positive and negative values, and thus it may not be an efficient measure to compare paths or systems. The power or energy ratios can be further defined. For example, the dissipated power ratios are Π_S/Π_{Tot}, Π_P/Π_{Tot} and Π_R/Π_{Tot}.

Next, the time-averaged potential energy is estimated for all spring and damper (massless) sub-systems based on Eq. (7). For instance, the potential energy into the receiver-grounding path is $E_{k,\mathrm{Rg}} = -\mathrm{Re}[X_R^* F_{\mathrm{Rg}}]/2$, and the potential energy of the ith path is $E_{k,i} = \mathrm{Re}\left[\left(X_S^* - X_i^*\right)F_{iS}\right]/2 + \mathrm{Re}\left[\left(X_R^* - X_i^*\right)F_{iR}\right]/2$. Fig. 9(a) compares paths using the potential energy ratios, defined for the ith path as $E_{k,i}/E_{k,P}$, where $E_{k,P} = \sum_{i=1}^{3} E_{k,i}$. In general, the ratio spectra show the path rank order more clearly, especially at the resonant frequencies (e.g. at 49 Hz); compare Fig. 9 with Fig. 8.

Finally, the time-averaged kinetic energy of each inertial body (B) is calculated from $E_{m,B} = M_B|V_B|^2/2$. Fig. 9(b) compares paths in terms of the kinetic energy ratios, defined as $E_{m,i}/E_{m,P}$, where $E_{m,P} = \sum_{i=1}^{3} E_{m,i}$. From Fig. 9(a) and (b), the path rank order is: Path 1 (dominant), 2, and 3 (least dominant) over lower and higher frequency ranges. This agrees with the order of path stiffness and mass values, respectively.

6. Path disconnect and connect methods for massless path system

We start with the simplest two degrees-of-freedom system of Fig. 2(a) with the parameters of Table 1 (without path masses). Since the path masses are negligible, we should be able to find some relationship between the α and β schemes of Fig. 3. Note that for a massless path model the SF and RF disconnect methods (see Section 2, paragraph 3 for definitions) of Fig. 3(c) are essentially the same as the CM disconnect method. The mobility matrix $\mathbf{Y}$ for the two degrees-of-freedom system of Fig. 2 is

$$\mathbf{Y}_{\mathrm{All}} = \frac{\mathrm{j}\omega}{\det \mathbf{Z}_{\mathrm{All}}} \begin{pmatrix} -\omega^2 m_R + \tilde{k}_{P_T} + \tilde{k}_R & \tilde{k}_{P_T} \\ \tilde{k}_{P_T} & -\omega^2 m_S + \tilde{k}_{P_T} + \tilde{k}_S \end{pmatrix}, \tag{40}$$

where $\det \mathbf{Z}_{\mathrm{All}} = \left(-\omega^2 m_S + \tilde{k}_{P_T} + \tilde{k}_S\right)\left(-\omega^2 m_R + \tilde{k}_{P_T} + \tilde{k}_R\right) - \tilde{k}_{P_T}^2$, and $\tilde{k}_{P_T} = \tilde{k}_1 + \tilde{k}_2 + \tilde{k}_3$ are defined for the sake of brevity. Then, velocity amplitude vectors are given as follows, given the harmonic force within the source: $(V_S, V_R)^{\mathrm{T}}_{\mathrm{All}} = \mathbf{Y}_{\mathrm{All}}(F_S, 0)^{\mathrm{T}}$. Also, other mobility matrices for the disconnected path systems may be easily found by modifying Eq. (40). Now, consider two types of insertion loss terms. First, find the insertion loss (in dB) based on V_R (and thus Y_R), and then calculate this insertion loss based on F_{RP} (total force transmitted to the receiver through all connected paths). Both expressions are found to be identical, as shown below, for the α or β scheme with the CM disconnect method:

$$\mathrm{IL}_{Y_R,\mathrm{CM}} = \mathrm{IL}_{F_{RP},\mathrm{CM}} = 20\log\left|\frac{\tilde{k}_{P_T}\det \mathbf{Z}_{\mathrm{CM}}}{\tilde{k}_e \det \mathbf{Z}_{\mathrm{All}}}\right|, \tag{41}$$

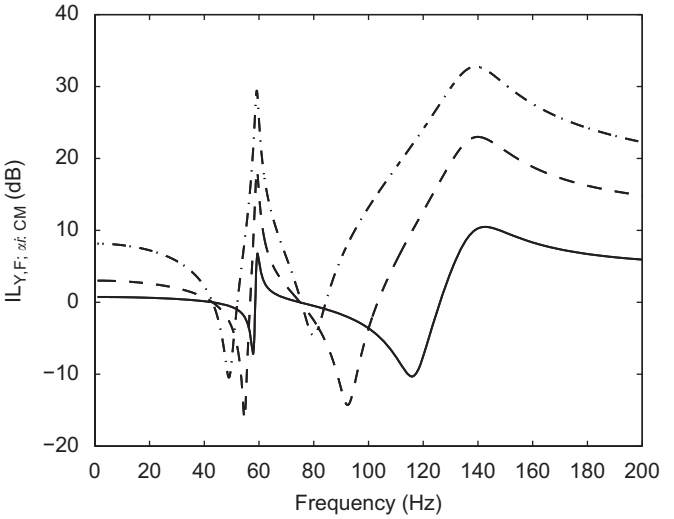

Fig. 10. Insertion loss spectra (based on the receiver mobility or force transmitted to the receiver given $\mathrm{IL}_{Y_R,\mathrm{CM}} = \mathrm{IL}_{F_{RP},\mathrm{CM}}$) using the α scheme for the two degrees-of-freedom system of Fig. 2(a). Key: ——, α scheme for Path 1; – – – –, α scheme for Path 2; · – · – · –, α scheme for Path 3.

where $\det \mathbf{Z}_{\mathrm{CM}} = \left(-\omega^2 m_S + \tilde{k}_e + \tilde{k}_S\right)\left(-\omega^2 m_R + \tilde{k}_e + \tilde{k}_R\right) - \tilde{k}_e^2$. In the subsequent expressions, the $\tilde{k}_e$ symbol refers to both α and β schemes by one expression. Here, $\tilde{k}_e$ is defined as $\tilde{k}_e = \tilde{k}_i$ for the α scheme for the ith path, but $\tilde{k}_e = \tilde{k}_{P_T} - \tilde{k}_i$ for the β scheme for the ith path. Both of the equations in Eq. (41) are plotted in Fig. 10, which confirms the identity. Fig. 10 also shows a more clear path rank order that is consistent with other measures (discussed again in Section 8). Next, we consider the transmissibility (TR) with the CM and RG disconnect methods since they are identical:

$$\mathrm{TR}_{\mathrm{CM}} = \mathrm{TR}_{\mathrm{RG}} = \left|\frac{\tilde{k}_e}{-\omega^2 m_R + \tilde{k}_e + \tilde{k}_R}\right|. \tag{42}$$

For the SG disconnect method of Fig. 3(c), three specific relations are found in terms of insertion loss based on motion transmissibility. From $\mathrm{TR}_{\mathrm{SG}} = \left|\tilde{k}_e/(-\omega^2 m_R + \tilde{k}_{P_T} + \tilde{k}_R)\right|$, $\mathrm{IL}_{\mathrm{TR;\ SG}}$ is now given as follows in terms of complex-valued stiffness terms:

$$\mathrm{IL}_{\mathrm{TR;SG}} = 20\log_{10}\left|\frac{\tilde{k}_{P_T}}{\tilde{k}_e}\right|. \tag{43}$$

First, Eq. (43) explains that $\mathrm{IL}_{\mathrm{TR;\ SG}}$ is governed by the storage stiffness in lower frequency regime and by the viscous damping in higher frequency regime, as given by the following asymptotic approximations:

$$\mathrm{IL}_{\mathrm{TR;SG}} \approx 20\log_{10}\frac{k_{P_T}}{k_e} \text{ at lower } \omega, \quad \mathrm{IL}_{\mathrm{TR;SG}} \approx 20\log_{10}\frac{c_{P_T}}{c_e} \text{ at higher } \omega. \tag{44a, 44b}$$

In particular, we observe that there is a transition regime in the $\mathrm{IL}_{\mathrm{TR;\ SG}}$ spectrum where the system resonances would dominate. Second, by observing the following fundamental relation $\tilde{k}_i/\tilde{k}_{P_T} + (\tilde{k}_{P_T} - \tilde{k}_i)/\tilde{k}_{P_T} = 1$, we derive an analytical relationship $10^{-\mathrm{IL}_{\mathrm{TR};\alpha i:\mathrm{SG}}/20} + 10^{-\mathrm{IL}_{\mathrm{TR};\beta i:\mathrm{SG}}/20} = 1$ from Eq. (43). Thus the following correlation between the α and β schemes, for the system of Fig. 2(a), is found as

$$\mathrm{IL}_{\mathrm{TR};\alpha i:\mathrm{SG}} = -20\log_{10}\left[1 - 10^{-\mathrm{IL}_{\mathrm{TR};\beta i:\mathrm{SG}}/20}\right], \tag{45a}$$

$$\mathrm{IL}_{\mathrm{TR};\beta i:\mathrm{SG}} = -20\log_{10}\left[1 - 10^{-\mathrm{IL}_{\mathrm{TR};\alpha i:\mathrm{SG}}/20}\right]. \tag{45b}$$

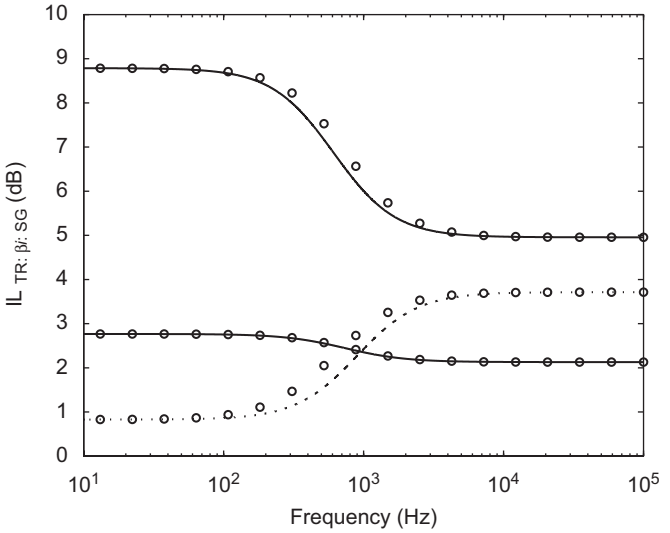

Fig. 11. Insertion loss spectra based on motion transmissibility (TR) using the β scheme for the two degrees-of-freedom system of Fig. 2(a). Key: ——, β scheme for Path 1 Eqs. (43) or (46b); – – – –, β scheme for Path 2 Eqs. (43) or (46b); · – · – · –, β scheme for Path 3 Eqs. (43) or (46b); ○, estimated by the $\alpha-\beta$ correlation Eq. (45b).

Third, when the individual path mobility is defined as $Y_i^P = \mathrm{j}\omega/\tilde{k}_i$, the combined (total) mobility of 3 (or more) parallel massless paths is $1/Y_T = \sum_i 1/Y_i^P$. Thus, Eq. (43) may be expressed as

$$\mathrm{IL}_{\mathrm{TR};\alpha i:\mathrm{SG}} = 20\log_{10}\left|\frac{1/Y_{P_T}}{1/Y_i^P}\right|, \quad \mathrm{IL}_{\mathrm{TR};\beta i:\mathrm{SG}} = 20\log_{10}\left|\frac{1/Y_{P_T}}{1/Y_{P_T} - 1/Y_i^P}\right|. \tag{46a, 46b}$$

Fig. 11 is plotted over a broad frequency range to show the distinct frequency regimes given by Eq. (44), and compares specific relations of Eqs. (45) and (46) with the direct estimation (43). The formulation with individual path mobilities (46) gives almost identical results (with no visible error) in Fig. 11 with Eq. (43), but the $\alpha-\beta$ scheme correlation (45) deviates from them only in the transition regime (approximately from 100 to 3000 Hz) where resonances dominate. Deviations show that the path masses must be included for improved calculations.

The experimental system of Fig. 2(b) was developed to validate the analytical formulation. Accordingly, the steel source and receiver bodies were chosen to be significantly heavier than the aluminum path rods. The visco-elastic isolators were placed at the source end. In order to experimentally find the relations given by Eqs. (43)–(46), the grounding condition (SG) is implemented by installing a large mass at the end of that path. Measured $\mathrm{IL}_{\mathrm{TR}}$ spectra for the β scheme with the SG disconnect method are compared in Fig. 12 with theoretical predictions. Experimental results reveal some more peaks that are related to the resonances of the sub-systems, such as the receiver and source beams, which are not modeled by the two degrees-of-freedom system. A larger error occurs in the stiffer path system, but the softest path system is well approximated by a straight line. Thus the massless path approximation has been found to be valid over the lower frequency range. This experimental example demonstrates that the path rank ordering process becomes much clearer in this specific case.

7. Path disconnect and connect methods for a system with path masses

Over a wider frequency range, the path masses cannot be ignored and we go back to the five degrees-of-freedom system of Fig. 1 with assumed $m_1 = 0.15$, $m_2 = 0.10$ and $m_3 = 0.07$ (kg), already used in the studies of Sections 4 and 5. The mobility expression is given as $\mathbf{Y} = \mathrm{j}\omega\mathbf{Z}^{-1}(1,0,0,0,0)^{\mathrm{T}}$, where $\mathbf{Z}$ is the dynamic stiffness matrix of the five degrees-of-freedom system. All path measures of Section 3 are then calculated. Fig. 13(a)

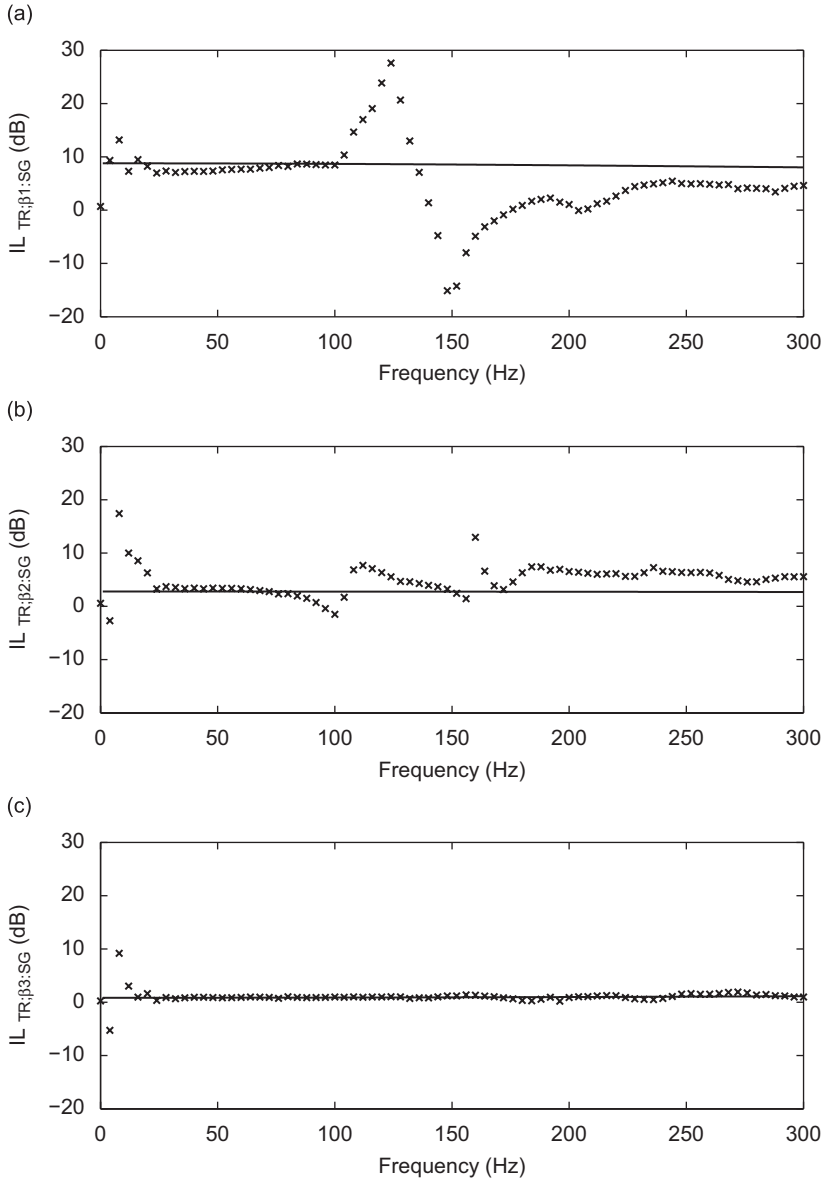

Fig. 12. Insertion loss spectra based on TR using the β scheme with SG disconnect method for the two degrees-of-freedom system of Fig. 2(a) or (b). (a) β scheme for Path 1; (b) β scheme for Path 2; (c) β scheme for Path 3. Key: ——, theory; x, experiment. SG: disconnect on the source side and ground the end.

shows the effect of path masses on the receiver mobility. Observe that two resonances of the five degrees-of-freedom system are not clear due to the relatively high damping. Further, Fig. 13(b) shows the individual path mobility Y_1^P (for Path 1), which clearly shows a resonance peak introduced by the mass of Path 1.

The specific relations given by Eqs. (41) and (42) are extended to the five degrees-of-freedom system for a more generic formulation. First, taking advantage of the mathematical cancellation effects when the insertion loss is estimated, define the path modification ratios (Σ) based on receiver velocity (V_R) and mobility (Y_R), force from/to receiver grounds (F_{Rg}), time-averaged kinetic ($E_{m,R}$), potential ($E_{k,R}$) and Lagrangian (L_R) energies and dissipated power (Π_R) in receiver. Such ratios result in the following insertion loss (in dB) identities.

$$\mathrm{IL}_{V_R} = \mathrm{IL}_{Y_R} = \mathrm{IL}_{F_{\mathrm{Rg}}} = \mathrm{IL}_{E_{m,R}} = \mathrm{IL}_{E_{k,R}} = \mathrm{IL}_{L_R} = \mathrm{IL}_{\Pi_R}, \tag{47a}$$

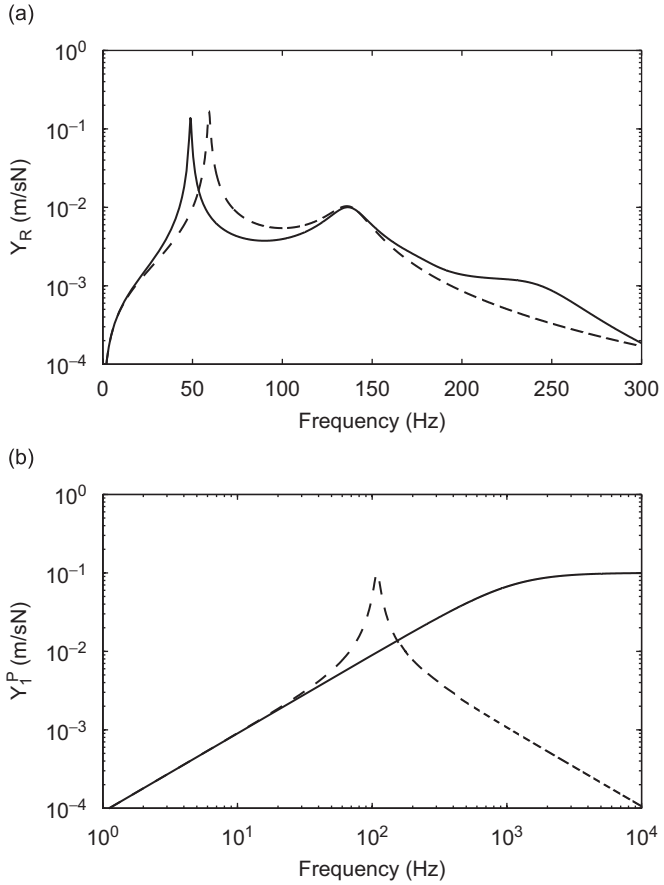

Fig. 13. Mobility magnitude spectra. (a) Receiver mobility; (b) individual mobility of Path 1. Key: (a) ——, five degrees-of-freedom system of Fig. 1; – – – –, two degrees-of-freedom system of Fig. 2. (b) ——, mobility of massless Path 1; – – – –, mobility of Path 1 with m_1.

where

$$\Sigma_{\alpha\beta} = \frac{V^2_{R,\mathrm{All}}}{V^2_{R,\alpha\beta}} = \frac{Y^2_{R,\mathrm{All}}}{Y^2_{R,\alpha\beta}} = \frac{F^2_{Rg,\mathrm{All}}}{F^2_{Rg,\alpha\beta}} = \frac{E_{m,R,\mathrm{All}}}{E_{m,R,\alpha\beta}} = \frac{E_{k,R,\mathrm{All}}}{E_{k,R,\alpha\beta}} = \frac{L_{R,\mathrm{All}}}{L_{R,\alpha\beta}} = \frac{\Pi_{R,\mathrm{All}}}{\Pi_{R,\alpha\beta}}. \tag{47b}$$

Here, the denominator could refer to any of the five disconnect methods for the α or β scheme in Fig. 3. These identities could permit a simplified and consistent comparison of paths.

Next, the specific relation of motion transmissibility given in Eq. (42) is extended as

$$\mathrm{TR}_{\mathrm{CM}} = \mathrm{TR}_{\mathrm{RG}} = \mathrm{TR}_{\mathrm{RF}}. \tag{48}$$

We analytically prove the above for the five degrees-of-freedom system of Fig. 1. Consider a generic translational system of dimension N where the input and output are at the first and the last (Nth) degree-of-freedom, respectively. Then, the velocity amplitude vector is given by

$$\mathbf{V} = \mathrm{j}\omega\mathbf{Z}^{-1}\mathbf{F} = \frac{\mathrm{j}\omega}{\det\,\mathbf{Z}} \begin{pmatrix} z^c_{1,1} & \cdots & z^c_{N,1} \\ \vdots & & \vdots \\ z^c_{1,N} & \cdots & z^c_{N,N} \end{pmatrix} \begin{pmatrix} F_S \\ 0 \\ \vdots \end{pmatrix}, \tag{49}$$

where $z^c_{i,j} = (-1)^{i+j}\mathrm{minor}|Z_{i,j}|$ is the co-factor of $z_{i,j}$, and $\mathrm{minor}|Z_{i,j}|$ is the minor of $\mathbf{Z}$ with respect to the ith row and the jth column. Note that motion transmissibility (TR) is the ratio of two velocity magnitudes, but purely from a mathematical view point, TR is the ratio of the corresponding two co-factors for a single input,

single output system:

$$\mathrm{TR} = \frac{V_R}{V_S} = \frac{z^c_{1,N}}{z^c_{1,1}}. \tag{50}$$

In order to reduce the amount of calculation for Eq. (50), notice that $z^c_{1,1}$ and $z^c_{1,N}$ share a major part of their determinants. Thus, we could reduce the calculation by expanding the determinants about the non-covalent columns as

$$z^c_{1,1} = z_{2,N}(-1)^{1+(N-1)}\mathrm{minor}\left|Z^S_{z_{2,N}}\right| + \cdots + z_{N,N}(-1)^{2(N-1)}\mathrm{minor}\left|Z^S_{z_{N,N}}\right|, \tag{51a}$$

$$z^c_{1,N} = (-1)^{1+N}\left[z_{2,1}(-1)^{1+1}\mathrm{minor}\left|Z^R_{z_{2,1}}\right| + \cdots + z_{N,1}(-1)^{(N-1)+1}\mathrm{minor}\left|Z^S_{z_{N,1}}\right|\right], \tag{51b}$$

where $\mathbf{Z}^S$ and $\mathbf{Z}^R$ are the sub-matrices of $\mathbf{Z}$ formed by excluding the first row and the first column, and the first row and the Nth column, respectively. The minor$\left|Z^S_{z_{i,j}}\right|$ is with respect to the row and the column where the component z_{ij} exists. Here, note that minor$\left|Z^S_{z_{i,N}}\right| = \mathrm{minor}\left|Z^R_{z_{i,1}}\right| (= g_i)$ for $i = 2,\ldots,N$ since they are the common to $z^c_{1,1}$ and $z^c_{1,N}$. Then, the ratio of $z^c_{1,N}$ to $z^c_{1,1}$ is written as

$$\mathrm{TR} = \frac{z^c_{1,N}}{z^c_{1,1}} = \frac{\sum_{i=2}^{N}(-1)^{i+1}z_{i,1}g_i}{\sum_{i=2}^{N}(-1)^{i}z_{i,N}g_i}, \tag{52}$$

where $z^c_{1,1} = \sum_{i=2}^{N}(-1)^{N+i}z_{i,N}g_i$ and $z^c_{1,N} = \sum_{i=2}^{N}(-1)^{N+1+i}z_{i,1}g_i$. Eq. (52) can simplify the calculation of Eq. (50). For example, the g_i terms for the β scheme for Path 1 (with the RG or RF disconnect method) of the five degrees-of-freedom system are:

$$\begin{cases} g_{2,\,\beta 1:\mathrm{RG}} = 0, \\ g_{3,\,\beta 1:\mathrm{RG}} = \tilde{k}_{2R}\left(\tilde{k}_1 - \omega^2 m_1\right)\left(\tilde{k}_3 - \omega^2 m_3\right), \\ g_{4,\,\beta 1:\mathrm{RG}} = -\tilde{k}_{3R}\left(\tilde{k}_1 - \omega^2 m_{P1}\right)\left(\tilde{k}_2 - \omega^2 m_2\right), \\ g_{5,\,\beta 1:\mathrm{RG}} = \left(\tilde{k}_1 - \omega^2 m_1\right)\left(\tilde{k}_2 - \omega^2 m_2\right)\left(\tilde{k}_3 - \omega^2 m_3\right), \end{cases} \quad \begin{cases} g_{2,\,\beta 1:\mathrm{RF}} = 0, \\ g_{3,\,\beta 1:\mathrm{RF}} = \tilde{k}_{2R}\left(\tilde{k}_{1S} - \omega^2 m_1\right)\left(\tilde{k}_3 - \omega^2 m_3\right), \\ g_{4,\,\beta 1:\mathrm{RF}} = -\tilde{k}_{3R}\left(\tilde{k}_{1S} - \omega^2 m_1\right)\left(\tilde{k}_2 - \omega^2 m_2\right), \\ g_{5,\,\beta 1:\mathrm{RF}} = \left(\tilde{k}_{1S} - \omega^2 m_1\right)\left(\tilde{k}_2 - \omega^2 m_2\right). \end{cases} \tag{53}$$

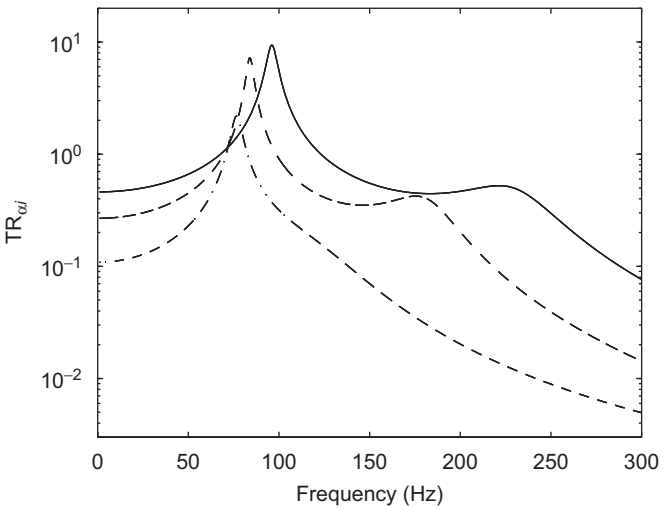

Fig. 14. Motion transmissibility (TR) spectra using the α scheme with CM, RF or RG disconnect method in the system of Fig. 1. Key: ——, α scheme for Path 1; – – – –, α scheme for Path 2; – · – · –, α scheme for Path 3. See Fig. 3 for the meaning of CM, RF and RG methods. (Each line represents 3 lines corresponding to CM, RF or RG disconnect methods.)

Here, $\tilde{k}_3 = \tilde{k}_{3S} + \tilde{k}_{3R}$ is defined as well. By additionally defining $g'_3 = \tilde{k}_{2R}(\tilde{k}_3 - \omega^2 m_3)$, $g'_4 = -\tilde{k}_{3R}(\tilde{k}_2 - \omega^2 m_2)$ and $g'_5 = (\tilde{k}_2 - \omega^2 m_2)(\tilde{k}_3 - \omega^2 m_3)$, the motion transmissibility is given as

$$\mathrm{TR}_{\beta 1:\mathrm{RG}} = \mathrm{TR}_{\beta 1:\mathrm{RF}} = \frac{\tilde{k}_{2S} g'_3 - \tilde{k}_{3S} g'_4}{-\tilde{k}_{2R} g'_3 + \tilde{k}_{3R} g'_4 + (\tilde{k}_{2R} + \tilde{k}_{3R} + \tilde{k}_R - \omega^2 m_R) g'_5}. \tag{54}$$

Since the CM disconnect method reduces the dimension of the system, $\mathrm{TR}_{\beta 1:\mathrm{CM}}$ may be directly calculated from Eq. (50) and then using the identity relation:

$$\mathrm{TR}_{\beta 1:\mathrm{CM}} = \mathrm{TR}_{\beta 1:\mathrm{RG}} = \mathrm{TR}_{\beta 1:\mathrm{RF}}. \tag{55}$$

The motion transmissibility expressions for the other five α or β schemes could be derived in the same way, which will finally prove Eq. (48). As a computational proof of Eq. (48), motion transmissibility spectra for the α scheme are shown in Fig. 14. Observe that the three disconnect methods CM, RF and RG give identical spectra for the α scheme (when applied to Paths 1, 2 and 3).

Table 3
Spectrally averaged insertion loss (IL) values in dB based on the receiver mobility (Y_R) and motion transmissibility (TR) for the α and β schemes for the five degrees-of-freedom system

Disconnect method	Insertion loss (dB)	Spectrally averaged value					
		α scheme			β scheme		
		Path 1	Path 2	Path 3	Path 1	Path 2	Path 3
CM	IL_Y	3.4	15.1	28.9	14.0	2.3	0.1
	$\mathrm{IL}_{\mathrm{TR}}$*	2.4	14.2	27.5	13.3	2.0	0.2
SG	IL_Y	6.6	14.5	28.2	13.5	4.7	1.0
	$\mathrm{IL}_{\mathrm{TR}}$	3.6	13.6	26.9	12.6	2.6	0.6
RG	IL_Y	8.9	17.9	29.2	15.8	6.4	1.5
	$\mathrm{IL}_{\mathrm{TR}}$*	2.4	14.2	27.5	13.3	2.0	0.2
SF	IL_Y	6.9	18.8	31.9	17.4	5.7	0.2
	$\mathrm{IL}_{\mathrm{TR}}$	10.1	17.0	29.9	15.0	8.4	1.3
RF	IL_Y	5.1	17.9	30.6	16.4	4.1	0.3
	$\mathrm{IL}_{\mathrm{TR}}$*	2.4	14.2	27.5	13.3	2.0	0.2

Various disconnect methods are shown in Fig. 3. Here, * indicates the identities of Eq. (48).

Table 4
Spectrally averaged insertion loss (IL) values in dB based on the receiver mobility (Y_R) and motion transmissibility (TR) for the α and β schemes for the two degrees-of-freedom system of Fig. 2(a)

Disconnect method	Insertion loss (dB)	Spectrally averaged value					
		α scheme			β scheme		
		Path 1	Path 2	Path 3	Path 1	Path 2	Path 3
CM	IL_Y	4.8	14.8	23.6	11.3	3.1	0.6
	$\mathrm{IL}_{\mathrm{TR}}$*	4.6	14.0	22.8	10.6	3.0	0.8
SG	IL_Y	5.2	12.2	21.6	9.4	3.7	1.0
	$\mathrm{IL}_{\mathrm{TR}}$	4.0	11.4	19.1	8.5	2.7	0.9
RG	IL_Y	8.2	16.7	24.2	14.2	6.0	1.5
	$\mathrm{IL}_{\mathrm{TR}}$*	4.6	14.0	22.8	10.6	3.0	0.8

Here, * indicates the identities of Eq. (42).

Table 5
Spectrally averaged values of absolute path measures for the five degrees-of-freedom system (Fig. 1)

Absolute path measure (units)	Spectrally averaged value {path rank}		
	Path 1	Path 2	Path 3
Mean-square velocity $0.5\|V_i\|^2$ ($\mu m^2/s^2$)	72.7 {3}	76.8 {2}	90.7 {1}
Upper path force $-\tilde{k}_{iS}(X_i - X_S)$ (N)	0.502 {1}	0.232 {2}	0.105 {3}
Lower path force $-\tilde{k}_{iR}(X_i - X_R)$ (N)	0.590 {1}	0.234 {2}	0.102 {3}
Dissipated power from Eq. (42a) (μW)	307 {1}	150 {3}	284 {2}
Dissipated power ratio Π_i/Π_P (%)	45.7 {1}	19.4 {3}	34.8 {2}
Kinetic energy $0.5M_i\|V_i\|^2$ (μJ)	10.9 {1}	7.68 {2}	6.34 {3}
Kinetic energy ratio $E_{m,i}/E_{m,P}$ (%)	55.4 {1}	30.7 {2}	13.9 {3}
Potential energy from Eq. (47) (μJ)	5.19 {1}	2.61 {2}	1.67 {3}
Potential energy ratio $E_{m,i}/E_{m,P}$ (%)	63.4 {1}	25.2 {2}	11.4 {3}
Lagrangian energy from Eq. (42b) (μJ)	5.72 {1}	5.07 {2}	4.67 {3}
Lagrangian energy ratio L_i/L_P (%)	58.2 {1}	29.0 {2}	12.8 {3}
Rank order based on relative path measures (from Tables 3 and 4)	{1}	{2}	{3}

All paths are connected for the calculations. Values within {} show the path rank orders.

8. Comparative path rank orders using alternative methods or measures

A summary of the relative measures (in terms of the insertion loss values averaged up to 300 Hz) for both the five and the two degrees-of-freedom systems are given in Tables 3 and 4, respectively. Observe a consistent path order: Path 1 is the most dominant and Path 3 is the least. This suggests that the α and/or β schemes could be successfully employed for simple (discrete translational type) systems, and that these schemes could provide a reasonable rank order, since a lower insertion loss (IL) value for the α scheme or a higher insertion loss level of the β scheme indicates that a particular path is more dominant. Further, the asymptotic regimes associated with the two degrees-of-freedom system show (see Fig. 11) that the above mentioned path order is valid in the lower frequency regime since it is governed by the path stiffness (k) values. In the higher frequency regime (governed by path damping (c) values) Paths 2 and 3 switch orders while Path 1 is still dominant.

Table 5 compares the absolute path measures in terms of spectrally averaged values (up to 300 Hz). It is observed that all path measures, except the mean-square velocity and dissipated powers, follow the path stiffness (k) order, as well as the ranking suggested by the relative measures of Tables 3 and 4. In fact, the dissipated power rank seems to mimic the path damping (c) orders, while the rank of mean-square velocity cannot be directly attributed to any one parameter. The energy-based path measures, especially the relative ones as shown in Fig. 15, show a clear path order even in the resonant frequency regions, where the absolute path measures yield somewhat inconsistent and measure-dependent path rank orders. One advantage of energy-based measures is that the energy or power ratio is meaningful, and their spectra tend to depict a clearer rank order as shown in Figs. 9, 15(a) and (b). Although the translational systems of this article do not require energy-based measures, the energy ratio and the insertion loss spectra are desirable from the path rank ordering perspective. Overall, we have found that the relative path measures yield a more consistent path rank order for the systems of Figs. 1 and 2. Although some inconsistency in the path rank order could exist given different path measures, the use of a relative path measure is recommended for a real-life system. Further study must be conducted to resolve the path rank inconsistency problem.

9. Conclusion

We employed a simple discrete system (with only translations) to critically assess the path identification issues and to analytically compare the rank orders that could be obtained by using the transfer path analysis and path disconnect methods. The path force estimation, which is the first stage in the transfer path analysis, is formulated by a direct (exact) method. Then four indirect, but yet exact, estimation methods are presented. Although it could be more efficient to employ the indirect methods that use the stiffness (F/X) type frequency

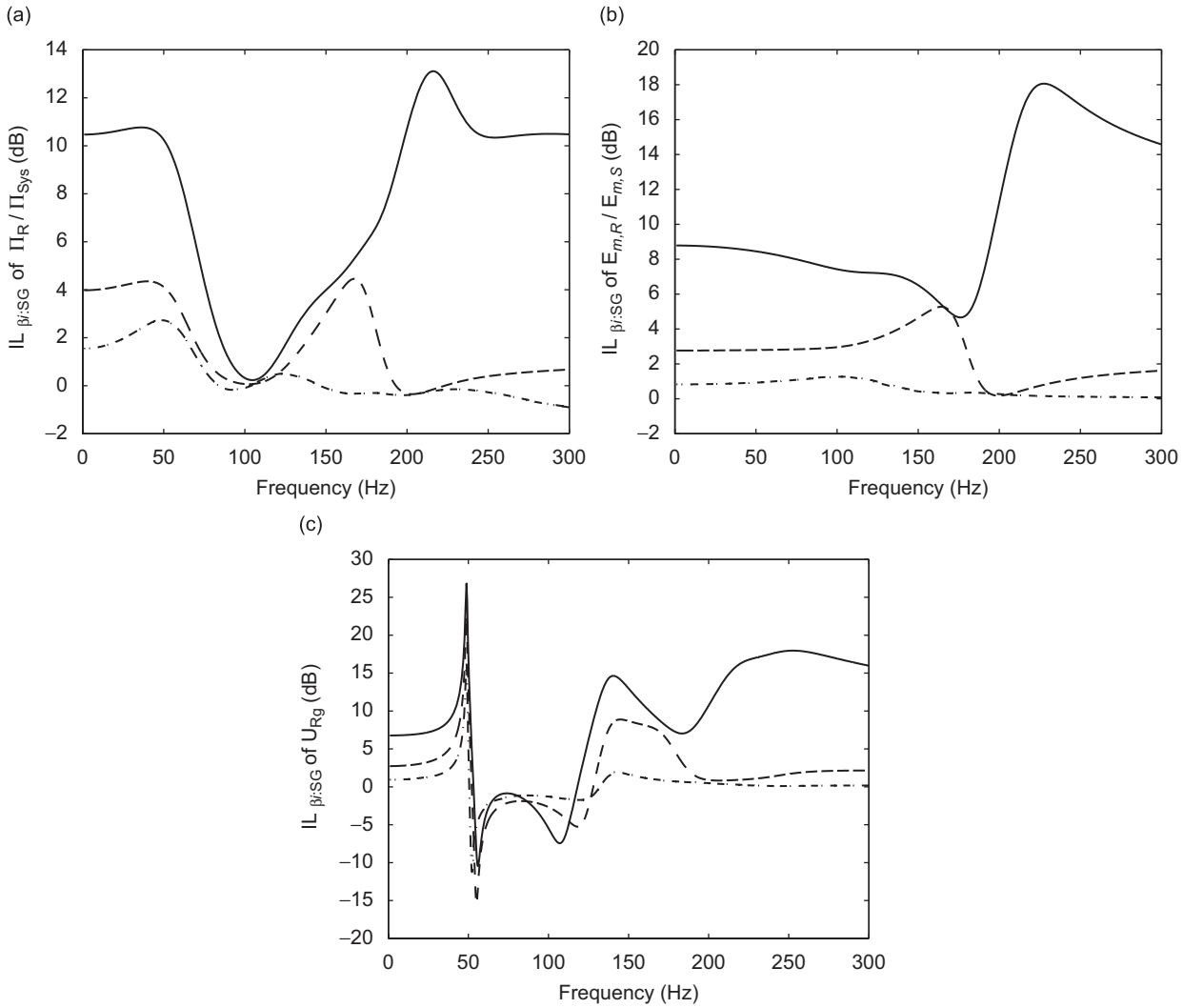

Fig. 15. Insertion loss (IL) spectra using the β scheme with SG disconnect method for the five degrees-of-freedom system (Fig. 1). (a) IL based on power ratio Π_R/Π_S. (b) IL based on the kinetic energy ratio $E_{m,R}/E_{m,S}$. (c) IL based on the potential energy $E_{k,\mathrm{Rg}}$. Key: ——, β scheme for Path 1; – – – –, β scheme for Path 2; $\cdot - \cdot - \cdot -$, β scheme for Path 3.

response functions with blocked boundary conditions, they are usually difficult to implement in practice. Thus, the compliance (X/F) type frequency response functions with free boundary conditions are utilized in experimental work. The four alternative indirect (yet exact) force formulations provide the theoretical basis while yielding further possibilities. The indirect force estimation methods enable the power or energy estimation of sub-systems in an easier but more accurate manner.

Next, we examined the conventional path disconnect methods and proposed the α and β schemes with five disconnect methods. For a system with massless paths, specific relations are found especially when the disconnected path is grounded at the source side (SG). For example, the $\alpha-\beta$ correlation described in Eq. (45) indicates that either the α or the β scheme could uniquely determine the other one. The massless path formulation has been validated by an experiment. The identities of transmissibility and insertion loss for the two degrees-of-freedom system (with massless paths) are next extended to the five degrees-of-freedom system with path masses, which are analytically and computationally proven. Such identities yield a simplified and yet consistent comparison of the paths. In those cases, when a particular disconnect method is difficult to implement, the identity relations present alternative means of the path quantification process.

Finally, we have compared the path rank orders using absolute and relative measures. In particular, both directional and energy-based path measures are used for the insertion loss calculations. While an almost consistent path order is found in our work, rotational motions should be included in a future study [32]. For the combined translational–rotational systems, energy-based measures (such as the ones given in this paper) would be more efficient. Also, further correlations between the α and β schemes should be numerically (or experimentally) sought in order to gain further insight into the path rank ordering procedures.

Acknowledgment

The Center for Automotive Research Industrial Consortium at The Ohio State University is gratefully acknowledged for supporting this research since Oct. 2001.

References

[1] R. Singh, S. Kim, Prediction of structure-borne noise transmission through multiple/multi-dimensional transfer paths, *Proceedings of the 2005 Noise and Vibration Emerging Methods Conference (NOVEM 2005)*, Saint Raphael, Cote d'Azure, France, April 2005 (Keynote Lecture).

[2] R. Singh, S. Kim, Examination of multi-dimensional vibration isolation measures and their correlation to sound radiation over a broad frequency range, *Journal of Sound and Vibration* 262 (3) (2003) 419–455.

[3] S. Kim, R. Singh, Multi-dimensional characterization of vibration isolators over a wide range of frequencies, *Journal of Sound and Vibration* 245 (2001) 877–913.

[4] P. Gardonio, S.J. Elliott, R.J. Pinnington, Active isolation of structural vibration on a multi-le-degree-of-freedom system, part I: the dynamics of the system, *Journal of Sound and Vibration* 207 (1) (1997) 61–93.

[5] P. Gardonio, S.J. Elliott, Passive and active isolation of structural vibration transmission between two plates connected by a set of mounts, *Journal of Sound and Vibration* 237 (2000) 483–511.

[6] J.S. Bendat, A.G. Piersol, *Engineering Applications of Correlation and Spectral Analysis*, Wiley, New York, 1980.

[7] A. Rust, I. Edlinger, Active path tracking—a rapid method for the identification of structure borne noise paths in vehicle chassis, *Proceedings of the Society of Automotive Engineers'Noise and Vibration Conference*, Grand Traverse, Michigan, USA, SAE Paper # 2001-01-1470, April 2001.

[8] A. Inoue, S. Kim, R. Singh, Comparative evaluation of structure-borne noise transfer paths in a laboratory experiment, *Noise Control Engineering Journal* 54 (6) (2006) 382–395.

[9] LMS International, Application Notes, *Transfer path analysis: the qualification and quantification of vibro-acoustic transfer paths*, 〈http://www.lmsintl.com/〉, 1995.

[10] F.X. Magrans, Method of measuring transmission paths, *Journal of Sound and Vibration* 74 (3) (1981) 321–330.

[11] J. Plunt, Examples of using transfer path analysis together with CAE-models to diagnose and find solutions for NVH problems late in the vehicle development process, *Proceedings of the Society of Automotive Engineers' Noise and Vibration Conference*, Grand Traverse, Michigan, USA, April 2005, SAE Paper # 2005-01-2508.

[12] J. Plunt, Strategy for transfer path analysis (TPA) applied to vibro-acoustic systems at medium and high frequencies, *Proceedings of the International Conference on Noise and Vibration Engineering (ISMA 23)*, Leuven, Belgium, September 16–18, 1998.

[13] M.A. Gehringer, Application of experimental transfer path analysis and hybrid FRF-based substructuring model to SUV axle noise, *Proceedings of the Society of Automotive Engineers'Noise and Vibration Conference*, Grand Traverse, Michigan, USA, April 2005, SAE Paper # 2005-01-1833, 2005.

[14] J.-H. Lee, K. Oh, Y.-S. Park, D.-H. Gwon, S.-K. Park, Transfer path analysis of structure-borne shock absorber noise in a passenger car, *Proceedings of the Society of Automotive Engineers' Noise and Vibration Conference*, Grand Traverse, Michigan, USA, April 2001, SAE Paper # 2001-01-1441.

[15] Y. Kanda, T. Saka, M. Fujikawa, K. Ando, I. Sako, I. Kawahara, Experimental transfer path analysis of gear whine, *Proceedings of the Society of Automotive Engineers' Noise and Vibration Conference*, Grand Traverse, Michigan, USA, April 2005, SAE Paper # 2005-01-2288.

[16] F. Haste, A. Nachimuthu, Calculating partial contribution using component sensitivity values: a different approach to transfer path analysis, *Proceedings of the Society of Automotive Engineers' Noise and Vibration Conference*, Grand Traverse, Michigan, USA, May 1999, SAE Paper # 1999-01-1693.

[17] A. Inoue, R. Singh, Errors associated with transfer path analysis when rotations are not measured, *Proceedings of the Society of Automotive Engineers' Noise and Vibration Conference*, St. Charles, Illinois, USA, May 2007, SAE Paper # 2007-01-2179, 2007.

[18] A.N. Thite, D.J. Thompson, The quantification of structure-borne transmission paths by inverse methods, part 1: improved singular value rejection methods, *Journal of Sound and Vibration* 264 (2003) 411–431.

[19] A.N. Thite, D.J. Thompson, The quantification of structure-borne transmission paths by inverse methods, part 2: use of regulation techniques, *Journal of Sound and Vibration* 264 (2003) 433–451.

[20] M.H.A. Janssens, J.W. Verheij, The use of an equivalent forces method for the experimental quantification of structural sound transmission in ships, *Journal of Sound and Vibration* 226 (2) (1999) 305–328.

[21] C.V. Kurmaniak, C.V. Karsen, W.R. Kelley, Application of indirect force estimation techniques to the automotive transfer case, *Proceedings of the Society of Automotive Engineers' Noise and Vibration Conference*, Grand Traverse, Michigan, USA, May 1999, SAE Paper # 1999-01-1764.
[22] M.Q. Wang, M.P. Sheng, J.C. Sun, The direct and indirect power flows of three non-conservatively series coupled oscillators, *Journal of Sound and Vibration* 212 (2) (1998) 231–251.
[23] J.C. Sun, C. Wang, Z.H. Sun, Power flow between three series coupled oscillators, *Journal of Sound and Vibration* 189 (2) (1996) 215–229.
[24] W.L. Liand, P. Lavrich, Prediction of power flows through machine vibration isolators, *Journal of Sound and Vibration* 224 (4) (1999) 757–774.
[25] Y.K. Koh, R.G. White, Analysis and control of vibrational power transmission to machinery supporting structures subject to a multi-excitation system, part II: vibrational power analysis and control schemes, *Journal of Sound and Vibration* 196 (1996) 469–494.
[26] N.M.M. Maia, J.M.M. Silva (Eds.), *Theoretical and Experimental Modal Analysis*, Research Studies Press, Somerset, UK, 1997.
[27] G. Pavic, The role of damping on energy and power in vibrating systems, *Journal of Sound and Vibration* 281 (2005) 45–71.
[28] S. Kim, R. Singh, Alternate methods for characterizing spectral energy inputs based only on driving point mobilities or impedances, *Journal of Sound and Vibration* 291 (2006) 604–626.
[29] J.W.S. Rayleigh, *Theory of Sound*, Dover Publications, New York, 1877 (re-issued 1945).
[30] G.B. Warburton, *The dynamical Behavior of Structures*, second ed., Pergamon International Library, New York, 1976.
[31] Y. Wang, T.C. Lim, M.L. Clapper, N.-M. Shiau, P. Braunwart, Y. Lee, Driveline NVH modeling applying a multi-subsystem spectral-based substructuring approach, *Proceedings of the Society of Automotive Engineers' Noise and Vibration Conference*, Grand Traverse, Michigan, USA, April 2005, SAE Paper # 2005-01-2300.
[32] C.M. Harris (Ed.), *Shock and Vibration Handbook*, fourth ed., McGraw Hill, New York, 1996.